Computer Methods in Applied Mechanics and Engineering 418 (2024) 116511

Contents lists available at ScienceDirect

Comput. Methods Appl. Mech. Engrg.

journal homepage: www.elsevier.com/locate/cma

A global–local meta-modelling technique for model updating

Gabriele Dessena[1,*], Dmitry I. Ignatyev, James F. Whidborne[**], Luca Zanotti Fragonara

School of Aerospace, Transport and Manufacturing, Cranfield University, College Road, Cranfield, MK43 0AL, Bedfordshire, UK

ARTICLE INFO

Dataset link: https://www.lanl.gov/projects/national-security-education-center/engineering/ei-software-download/index.php, https://doi.org/10.5281/zenodo.8406030

Keywords:
Kriging
Model updating
MTMAC
Structural Health Monitoring
Damage detection
Optimisation

ABSTRACT

The finite element model updating procedure of large or complex structures is challenging for engineering practitioners and researchers. Iterative methods, such as genetic algorithms and response surface models, have a high computational burden for these problems. This work introduces an enhanced version of the well-known Efficient Global Optimisation technique to address this issue. The enhanced method, refined Efficient Global Optimisation or rEGO, exploits a two-step refinement and selection technique to expand the global search capability of the original method to a global–local, or hybrid, search capability. rEGO is tested and validated on four optimisation test functions against the original methods and genetic algorithms with different settings. Good results in terms of precision and computational performance are achieved, so an application for model updating is sought. A penalty function for the finite element model updating is identified in residuals of the modified total modal assurance criterion. Finally, rEGO for finite element model updating is implemented on a hybrid, numerical and experimental, case study based on a well-known experimental dataset and on a higher dimension finite element model of a wing spar. Satisfactory results in terms of precision and computational performance are achieved when compared to the original methods and genetic algorithms, needing two orders of magnitude fewer evaluations and achieving comparable results in terms of precision.

1. Introduction

Finite Element Models (FEMs) are a fundamental tool for the design and analysis of engineering structures. However, out-of-the-box FEMs rarely match the behaviour of a system without tuning. The process of tuning a model to data obtained from an existing structure is known as FEM updating (FEMU) and for large, or complex structures the process can become lengthy and convoluted. Particularly, iterative processes driven by Evolutionary Algorithms (EAs) suffer this drawback. In this work, a novel global–local optimisation routine based on the Efficient Global Optimization (EGO) [1] and Kriging [2] is introduced to address this problem. The new technique draws on the advantages of meta-modelling to create an iterative routine for FEMU, which, in particular, can be applied for damage detection of mechanical systems. The method is first outlined and, then, validated against existing optimisation techniques on a selection of well-known test functions. Subsequently, a suitable goal function for FEMU is identified and, lastly, the method is used for the model updating and damage detection on the well-know three storey frame structure from the Engineering Institute at the Los Alamos National Laboratory (LANL) [3] and on larger FEM of a wing spar built in ANSYS Mechanical APDL. The goal of this paper is to introduce and validate a new surrogate-based optimisation technique which broadens the scope of EGO to global–local optimisation. The new technique needs to improve the precision and computational performance, particularly in the applications of interest: FEMU and damage detection.

* Corresponding author.
** Primary corresponding author.
E-mail addresses: gdessena@ing.uc3m.es, gabriele.dessena@cranfield.ac.uk (G. Dessena), j.f.whidborne@cranfield.ac.uk (J.F. Whidborne).
[1] Present address: Department of Aerospace Engineering, Universidad Carlos III de Madrid, Av. de la Universidad, 30, 28911 Leganés, Madrid, Spain.

https://doi.org/10.1016/j.cma.2023.116511
Received 20 February 2023; Received in revised form 15 July 2023; Accepted 2 October 2023
Available online 9 October 2023

A brief review of the application of FEMU for damage detection and a description of Kriging and EGO are given in Section 2. Section 3 introduces the newly developed technique, refined Efficient Global Optimisation (rEGO), its application to model updating is outlined in Section 4, a hybrid, numerical and experimental, case study on the three storey frame structure from the Engineering Institute at LANL is presented in Section 5 and the FEMU of the wing spar is shown in Section 6.

2. Methods

In this section the applications of FEMU for damage detection are recalled before introducing Kriging and EGO.

2.1. Model updating for damage detection

Model updating, intended as the calibration of FEMs using experimental data, is an established strategy within structural engineering [4]. Hence, the main goal of model updating is to establish a FEM representative of the actual system as much as possible. In fact, due to manufacturing, materials or modelling assumptions, an out-of-the-box FEM is rarely adequately coherent with its real counterpart [5]; for this reason, a growing interest in model updating is registered over the last three decades [6–9].

Apart from matching the behaviour of a model to a real structure, model updating can be used for damage detection, commonly referred to as Structural Health Monitoring (SHM) [10]. SHM is defined as the statistical pattern recognition strategy of damage in a system, by which operational capability or functionality is influenced. According to [11] this can be summarised in a four-point procedure:

1. Operational evaluation: such as a testing campaign;
2. Data acquisition and cleansing: data collection and processing from the test data;
3. Feature selection: defining what parameters or values are going to employ for the SHM task;
4. Statistical model development: assessing the structure by comparing the undamaged and current state.

A large number of SHM methods have been proposed [12]; however, the most prevalent are the vibration-based approaches, which can be further divided into direct [13] and indirect [14] methods. The former involves data obtained directly from tests, such as modal parameters or frequency response functions (FRFs), whereas the latter is the subject of this work, involving model-oriented methodologies known as model-based SHM. The underlying assumption of this approach is that a change in the parameters of the model between a baseline and a damaged scenario returns information on the presence, location, and severity of the damage [15]. Giving a thorough review of SHM is beyond the scope of this paper and the interested reader is referred to [16] for a general overview, to [12] for a summary on the state of industry implementation for SHM and to [15] for a review on iterative methods for SHM.

Model updating techniques can be divided into direct and indirect methods [15]. The former are efficient and accurate methods that use modal characteristics to update the FEMs. *Direct* methods include matrix updates [17], optimal matrix [18], error matrix [19] and eigenstructure assignment [20]. However, these methods are not particularly appealing for engineering practice, particularly damage detection, as they present several critical drawbacks: (i) they require very precise measurement of the structural vibration response, (ii) they are sensitive to noise, (iii) they cannot be used with truncated data and (iv) they may lose symmetry in the FEM matrix. With these preconditions, *indirect*, or iterative, methods are introduced. Firstly, it is beneficial to make a distinction based on the information used for the FEMU, which can be modal data (ω_n, ζ_n, and $\boldsymbol{\phi}_n$) or directly the structure response, either in time or frequency domain. Most commonly, modal parameters and frequency domain data are used. This work focuses on modal data-based FEMU.

The *indirect* FEMU methods can be divided into five subcategories: (i) sensitivity-based methods, (ii) response surface methods (RSMs), (iii) Bayesian and Monte Carlo methods, (iv) computational intelligence techniques, and (v) Evolutionary Algorithms (EAs) methods. The general rule for indirect methods is that there is a penalty, or goal, function to be minimised in order to update the model, generally based on frequency response [21] or modal parameters [22]. The distinction within the methods lies in the way this is obtained.

Sensitivity-based methods consider a system's measured response as a change in the initial FEM parameters and the aim is to minimise this difference with a penalty function. The main limitation of this approach is its constraint in detecting small-scale damage. Nevertheless, the method is widely employed in literature, e.g the work of [23] for heritage structures.

Bayesian–Monte Carlo methods are based on the probability distribution function built on a set of data, such as defined by Bayes' theorem. These methods have the drawbacks of high computational cost, due to the requirement of solving complex integrals, and of the prior knowledge of interval distributions of updating parameters [24]. Nevertheless, fruitful implementations are available in the literature, such as the work of [25].

Computational intelligence, or machine learning, model updating techniques take advantage of the fact that FEM model updating is an optimisation problem. The requirement for a large amount of data, as for any other machine learning problem, is the main drawback of this method. However, researchers have successfully applied the method in many instances. A prominent example is the work of [26], which treats online model updating for structural health monitoring.

Sometimes classified with the computational intelligence methods, EAs are regarded as an efficient method to solve highly nonlinear and multimodal problems [15]. This allows them to be accurate instruments for dealing with optimisation-driven FEMU. As stated in [27], the most prominent and employed EA technique is a genetic algorithm (GA) [28], which, however, was shown to have a major drawback for model updating [29]: the number of iterations needed is relatively high, when compared to other

techniques. This poses a problem when employing this methodology with complex or very large structures. Nevertheless, many applications of FEMU with EAs exist, such as the work of [30], which employed GAs to tune a FEM from modal data.

Lastly, the RSM is a statistically driven approach where a correlation is built between the input variables and response. A predefined goal or penalty function drives the response. While simple methods like polynomial functions can be used to draw the RSM, more advanced techniques are available, such as Kriging [2] and its RSM implementation, the Efficient Global Optimisation (EGO) [1]. A slightly modified version of EGO is used in [29] for FEMU, while [7] usees classical polynomial regression for the same scope. The main drawback of RSM for FEM is the application of statistical approximations with unknown parameters which may result in the ill-conditioning of the final model [24].

The reader interested in a more comprehensive review can refer to the book by [31] and the work by [6]. The reader particularly interested in *indirect* methods can refer to works of [15,24].

2.2. Kriging and the Efficient Global Optimisation

The idea behind meta-modelling is to create a response surface which mimics the relationship between a function, or problem, input variables and its output. RSMs obtain this goal by replacing the underlying implicit function of the original problem with an approximation model, traditionally a polynomial; hence, a computationally inexpensive function to evaluate [24]. However, more involved approaches exist that offer models with higher fidelity. One of these approaches, Kriging, is used in this work. The reader who is interested in a review and application of classical techniques is directed to the book in [24] and the work in [7].

Kriging originated in geostatistics, in the 1950s [2]; however, more recently it has seen multiple applications within engineering, particularly in design [32,33]. Nevertheless, applications for FEM model updating are scarce [29,34–36] and mostly do not take full advantage of surrogate-based optimisation, being mostly limited to response surface fitting. The main reason for the lack of applications in FEMU is because there is no real proof of convergence, in the sense that the obtained minimum could be far from the actual minimum [37]. However, this has longly [1] been deemed to be irrelevant when the meta-model is built *strategically* (following a workflow), such as for EGO. EGO can be defined as the strategic RSM implementation of Kriging and can be outlined as follows:

1. The design of experiment (DoE) is created in order to collect a large number of samples from the goal, or penalty, function in a strategic manner (usually LH);
2. Kriging is applied to the data obtained from the DoE, and a predictor is created.;
3. The RSM can be *strategically* updated with new results, such as computing the value of the expected minimum;
4. Iteratively moving between points 2 and 3 until convergence is achieved.

In fairness, the procedure could stop after point 2 is cleared. However, the approximated response at that stage is most likely not going to be accurate enough to exploit it, which is what EGO aims to do. The procedure starts with the DoE, which aims to evaluate the original function, or problem, at well-distributed points in the search space. The most prominent technique to obtain this is the Morris–Mitchell optimal Latin hypercube (LH) [38,39], which minimises the largest distance between any pair of points within the sample through an iterative procedure. This technique is considered to create the initial population, the DoE, within this work. General consensus [40] is that the initial sample should contain ten times as many points as there are variables in the problem. The interested reader can refer to the work by [41] for a broader review of sampling strategies.

Kriging is a stochastic meta-modelling technique that is based on the relationship between sample data (input) $\boldsymbol{X}$ and observed response (output) $\boldsymbol{Y}$ as follows:

$$\begin{aligned} &y_i(\boldsymbol{x}) = \boldsymbol{f}^T(\boldsymbol{x}_i)\boldsymbol{\beta} + z(\boldsymbol{x}_i), \quad \text{for} \quad i = 1, 2, \dots, n \\ &\text{with} \\ &\quad \boldsymbol{X} = \{\boldsymbol{x}_1, \boldsymbol{x}_2, \dots, \boldsymbol{x}_n\}^T, \quad \boldsymbol{Y} = \{y_1, y_2, \dots, y_n\}^T \end{aligned} \tag{1}$$

where $\boldsymbol{f}(\boldsymbol{x})$ is the polynomial vector of $\boldsymbol{x}$, $\boldsymbol{\beta}$ is the linear regression vector of the coefficients to be estimated and $z(\boldsymbol{x})$ represents the error as a stochastic process following a normal distribution, such as $N(0, \sigma^2)$ with a zero mean (μ) and standard deviation (σ). In order to estimate $z(\boldsymbol{x})$, a correlation model needs to be set. The most common model is Gaussian correlation [29]; hence the entries of the correlation matrix $\boldsymbol{R}$ can be built accordingly:

$$\boldsymbol{R}_{ij}(z(\boldsymbol{x}_i), z(\boldsymbol{x}_j)) = \exp\left(- \sum_{k=1}^{m} \theta_k \left| x_i^k - x_j^k \right|^2 \right) \tag{2}$$

where x_i^k are x_j^k the ith and jth elements of, respectively, $\boldsymbol{x}_i$ and $\boldsymbol{x}_j$, m is the number of variables and θ_k is the decay rate of correlation between the different variables, defined iteratively at each model implementation. At this point the likelihood function can be defined:

$$L = \frac{1}{(2\pi\sigma^2)^{m/2}|\boldsymbol{R}|^{1/2}} \exp\left[- \frac{(\boldsymbol{Y} - \boldsymbol{F}\boldsymbol{\beta})^T \boldsymbol{R}^{-1} (\boldsymbol{Y} - \boldsymbol{F}\boldsymbol{\beta})}{2\sigma^2} \right] \tag{3}$$

where $\boldsymbol{F}$ represents the matrix of $\boldsymbol{f}(\boldsymbol{x})$ for each point. If the maximum likelihood is considered [32], the following are defined:

$$\begin{aligned} &\hat{\boldsymbol{\beta}} = (\boldsymbol{F}^T \boldsymbol{R}^{-1} \boldsymbol{F})^{-1} \boldsymbol{F}^T \boldsymbol{R}^{-1} \boldsymbol{Y} \\ &\hat{\sigma}^2 = \frac{(\boldsymbol{Y} - \boldsymbol{F}\boldsymbol{\beta})^T \boldsymbol{R}^{-1} (\boldsymbol{Y} - \boldsymbol{F}\boldsymbol{\beta})}{n} \end{aligned} \tag{4}$$

The maximum likelihood can be expressed in a logarithmic way:

$$\ln(L) \approx -\frac{m}{2}\ln(\hat{\sigma}^2) - \frac{1}{2}\ln|\boldsymbol{R}| \tag{5}$$

At this stage, Eq. (5) is maximised via a GA to obtain the value of θ_k for the different variables.

The Kriging model is now built and the predictor for any point $\boldsymbol{x}_0$ can be defined as follows:

$$\hat{y}(\boldsymbol{x}_0) = \boldsymbol{f}^T(\boldsymbol{x}_0)\hat{\boldsymbol{\beta}} + \boldsymbol{r}^T(\boldsymbol{x}_0)\boldsymbol{R}^{-1}(\boldsymbol{Y} - \boldsymbol{F}\hat{\boldsymbol{\beta}}) \tag{6}$$

with $\boldsymbol{r}$ denoting the n-vector of correlations between the value $y(\boldsymbol{x}_0)$, at $\boldsymbol{x}_0$ and the error terms $y(\boldsymbol{x}_{0-n})$ at the previously sampled points, such that:

$$\boldsymbol{r}^T(x_0) = [R(\boldsymbol{x}_0, \boldsymbol{x}_1), \dots, R(\boldsymbol{x}_0, \boldsymbol{x}_n)] \tag{7}$$

After generating the initial model, an updating strategy has to be considered to increase the model's precision. Traditionally, the quantities such as the minimum of the model error are infilled (data points added to model); however, EGO [1] introduced the expected improvement (EI), which can be defined intuitively as the amount by which the minimum of the goal function can be improved if a point at a given location is filled. Also, it is, graphically, defined as the first moment of the area under the Gaussian distribution of the probability of finding a better minimum than the best-observed value [32]:

$$\begin{aligned} \mathrm{EI} = E[I(x)] = (y_{min} - \hat{y}(\boldsymbol{x}))\left[\frac{1}{2} + \frac{1}{2}\mathrm{erf}\left(\frac{y_{min} - \hat{y}(\boldsymbol{x})}{\hat{s}\sqrt{2}}\right)\right] + \\ + \hat{s}\frac{1}{\sqrt{2\pi}}\exp\left[\frac{-(y_{min} - \hat{y}(\boldsymbol{x}))^2}{2\hat{s}^2}\right] \end{aligned} \tag{8}$$

where $\hat{y}(\boldsymbol{x})$ is the model predicted value at $\boldsymbol{x}$, erf is the error function and $\hat{s}$ is the standard deviation, defined as the population standard deviation.

For deeper insights into the EI the interested reader is referred to [1,32]. The graphical definition of EI in Eq. (8) is considered within this work.

Summarising, *direct* methods for FEMU are not feasible in real operations; hence, resorting to *indirect* methods is imperative. Within this realm, drawbacks exist for all four subcategories. Moreover, the good track record of RSM in engineering design [33,42] makes them a suitable candidate to solve, with a novel implementation, its modest drawbacks. Given the aforementioned introduction of FEMU methods, SHM and meta-modelling, the aim of this work is to exploit the capabilities of RSM FEMU by introducing a new RSM, based on Kriging and EI, to improve the search performance in a global–local, or hybrid, sense for FEMU and damage detection applications.

3. The refined Efficient Global Optimisation

This section deals with the introduction of the newly developed meta-modelling technique, the rEGO, and with its numerical validation. First, the rEGO workflow and foundations are described, and then a numerical study, of four test functions, has the goal of establishing a general rule for the quantification of the first stopping criterion (ϵ_1) and comparing rEGO to the well-established EGO and GA for optimisation purposes.

3.1. Workflow

The main goal of rEGO is to enhance the search capability given by the standard EGO by implementing a global–local search capability,a partly successful attempt is found in [43], where however no formal study was carried out on the method's hyperparameters and its performance. The hyperparameters, in particular of ϵ_1, study in this work fully motivates and proves its contribution to the established EGO. The enhancement is achieved in two ways: refinement and selection. First of all, refinement is achieved at a global scale, by halving the search space, when good knowledge of the response surface is achieved. Then, at a local level, with a local convergence criterion, the second stopping criterion (ϵ_2), which is based on the Euclidean distance between the variables of proposed minima and the current best estimate (x_{dist}). The former is inspired by the design domain reduction method in [44,45], which aims to halve the search space near the known minimum after some condition is met, in a similar fashion to multi-objective optimisation [46] and Pareto fronts dominance [47]. In the application under scrutiny, the condition is related to the exploration of the response surface and, hence, to the ϵ_1 and the EI. Moreover, the latter is a common feature of optimisation algorithms and it is set as 10^{-4}, such that $\epsilon_2 = 10^{-4}$.

The refinement technique can be split into two separate tasks: exclusion and de-clustering. Exclusion is a direct consequence of the search space halving and consists in eliminating from the data pool the points which do not lie in the new search space. However, this is not sufficient in ensuring an efficient computation, as a cluster of points might have formed within the data pool. At this stage, de-clustering enters into action by ensuring points within the same cluster are excluded and only the middle point, in terms of variables' position in space, is left. This ensures the most efficient possible computation of the updated Kriging meta-model. In order to avoid convergence to local minima with few data points, a minimum requirement for the size of the data pool is created, in such a way that the ϵ_1 cannot be satisfied if the number of points is less than ten times the number of variables, which is the same principle driving initial sampling. In addition, two stopping criteria are defined. The first prescribes a refinement if, after 100 times

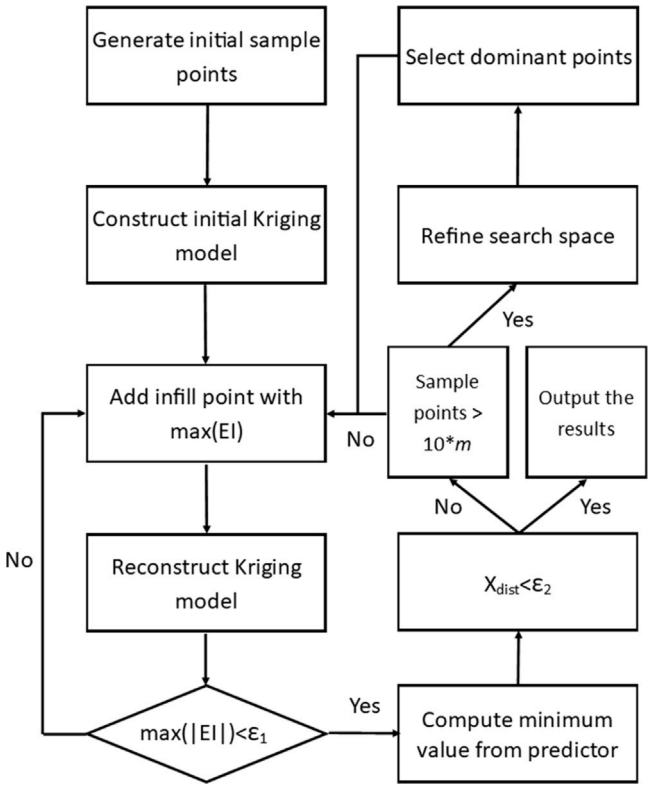

Fig. 1. rEGO workflow chart. m is the number of variables of the problem.

the number of variables ($m \times 100$) iterations, there has not been another refinement (ϵ_1 not reached), while the second criterion stops the optimisation when the minimum of the function has not improved (stall) after 100 times the number of variables ($m \times 100$) iterations.

The techniques mentioned above allow rEGo to become a global–local optimisation technique and improve the global-only capability of EGO. Now, the running algorithm if rEGO is outlined:

1. The initial population of size $10 \times m$, m is the number of variables, is computed using an LH for ;
2. The initial Kriging model is built as per Eq. (6);
3. The point where the maximum EI is found is computed and the Kriging model is updated. This process is known as infill;
4. The ϵ_1 is verified. If the condition is not met the process goes back to step 2;
5. The minimum location, with a GA, found from the predictor is computed;
6. If ϵ_2 is verified the algorithm terminates. Otherwise, the number of points is evaluated and if less than $10 \times m$, the process goes back to point 2.
7. The search space is refined and the dominant points are selected, de-clustering, and the algorithm iterates from step 2.

Steps 1 to 3 represent the left column of the rEGO diagram in Fig. 1 and frame the EGO algorithm first introduced in [1].

The critical part of the workflow is the definition of ϵ_1, linked to the EI. In theory, perfect convergence can be reached when $\hat{s} = 0$ of Eq. (8); nevertheless, when dealing with real data this is highly impracticable. However, in practice [1] suggests that a good convergence condition can be achieved for EI = 1% of the minimum of the function that is searched. If the condition is not satisfied, then the point with the maximum EI is infilled and the process iterates until convergence. The impracticability of the $\hat{s} = 0$ condition makes EGO less reliable in global search because an amount of uncertainty is postulated with the stopping criterion. In fact, in rEGO ϵ_1, as per EGO, is the measure of the global exploration of the response surface and, since a new method is proposed, it is improper to retain the value suggested in [1]. Hence, a numerical study, in the following subsection, investigates the relationship between EI and the algorithm's precision.

Within this work, the Design and Analysis of Computer Experiments (DACE) toolbox [48] is used to create the Kriging model and for de-clustering the data pool, for which its `dsmerge` function is employed. The EI function is retrieved from [49,50], while the optimal LH code is native to MATLAB, the `lhdesign` function. The authors' complete implementation and an introductory tutorial of rEGO can be found in a Cranfield Online Research Data entry linked in the Data Availability Statement.

Table 1
Test functions.

Function	Number of variables
Modified Branin [32]	2
Hartmann 4-D Function [52]	4
Rastrigin [53]	6
Styblinski–Tang [54]	8

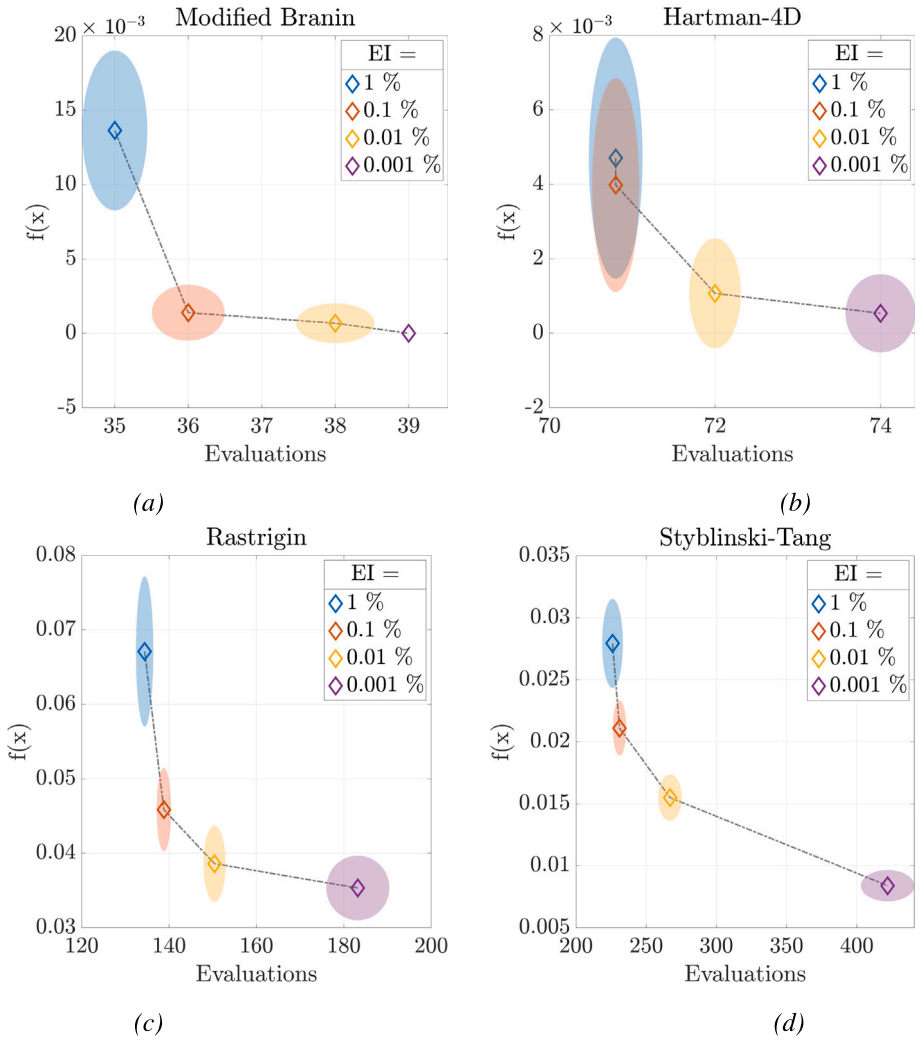

Fig. 2. Results of the numerical study concerning ϵ_1 and computational efficiency. The ellipses represent the uncertainty in terms of a 95% Confidence Interval (CI) over 100 realisations.

3.2. Numerical validation

In order to investigate the relationship between the EI and the precision of the algorithm, four optimisation test functions, presented in Table 1, have been selected and their inputs and outputs scaled between 0 and 1. The functions implementations are adapted from [51].

The ϵ_1 taken into consideration within this numerical study are EI = [1%, 0.1%, 0.01%, 0.001%]. Since the original EGO implementation considered 1% to be a suitable stopping criterion, only smaller values are considered. This study's main goal is to select a suitable EI value to be used as ϵ_1 within rEGO. The decision is based on the compromise between precision and computational effort, the number of functions evaluations to convergence. The results of this survey for the functions in Table 1 are presented in Fig. 2. The plots' ellipses represent the 95% Confidence Interval (CI) and the markers show the mean values, both over 100 realisations, intended as runs of the algorithm.

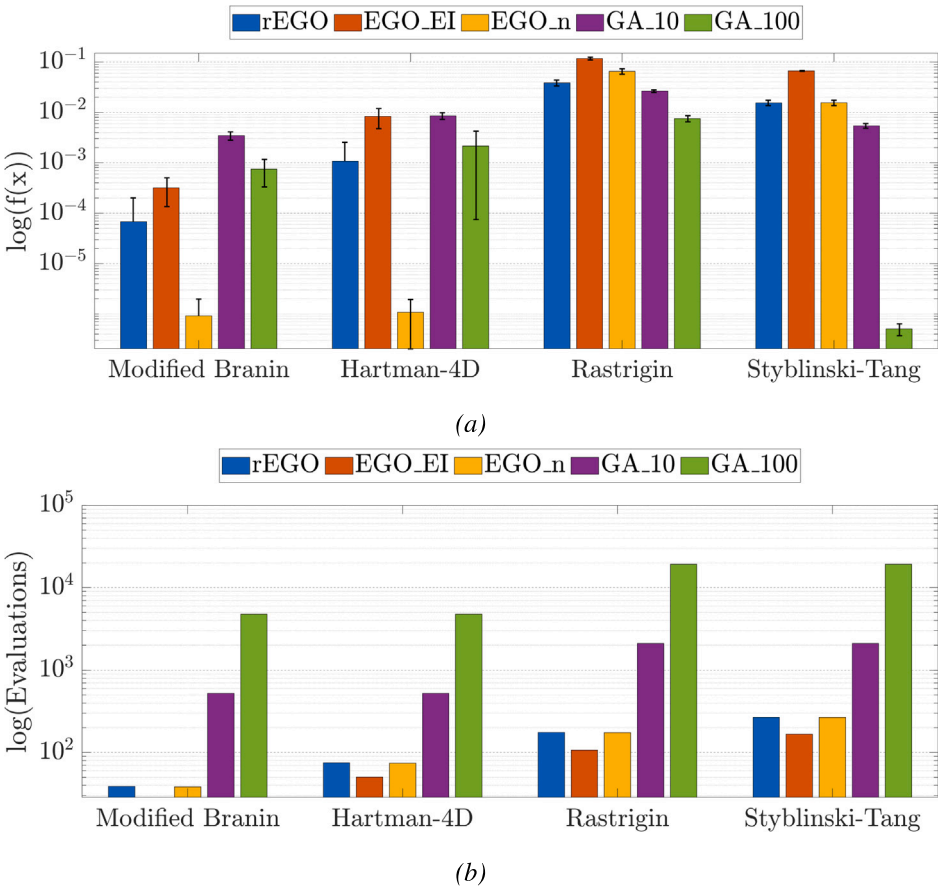

Fig. 3. Results of the numerical study concerning the objective, f(x), and computational efficiency, number of evaluations. The plots' error bars represent the 95% Confidence Interval (CI) over 100 realisations.

The statistical study is necessary for the random nature of the Kriging modelling. In all cases, the largest intervals for CI are observed for the highest EI value, 1%. This is somewhat expected as for a higher EI the knowledge of the response surface is more uncertain than smaller EIs. Nevertheless, this general rule does not apply for the number of evaluations. In fact, as clearly shown in Figs. 2(b)–2(d), for the smallest EI value (EI=0.001%) the largest uncertainty, in terms of computational effort, is found.

The highest and lowest proposed EI have two major drawbacks: the former's precision is notably worse than the others and the latter is the worst computationally; hence, they are excluded, leaving two potentially suitable values. Apart from the Modified Branin, the 0.01% value always offers a steep improvement in precision, in terms of both average value and smaller CI, than its larger counterpart. Even if the computational effort is larger for EI = 0.01%, when compared to EI = 0.1%, the difference is small, always within 10%. Finally, from a graphical consideration, only the EI = 0.01% value lies in what is called the knee of the Pareto front, which, for a two-objective problem like this, indicates a good compromise between the two objectives. Hence, the value of EI = 0.01% is selected as the ϵ_1 within this work and as the standard value for the rEGO algorithm.

After having established the two stopping criteria driving the rEGO search, it is pivotal to validate the new algorithm against existing techniques. The same test functions are evaluated by rEGO, EGO and GA 100 times (realisations) for statistical relevance. For rEGO, ϵ_1 is 0.01% and ϵ_1 is 10^{-4}, while for EGO two implementations are considered. One takes into consideration EI = 0.01% as the stopping criterion (EGO_EI) and the other with a maximum number of function evaluations equal to the average of rEGO's evaluations to convergence (EGO_n). This means that the evaluation budget for the four functions is set, respectively to 39, 75, 176, and 265. With respect to GAs, two sets of GAs are considered. One with a number of generations of 10 (GA_10) and the other of 100 (GA_100). All the other parameters are standard as per the `ga` function MATLAB implementation. For all strategies, the starting population is defined by an LH generating a number of points ten times the number of variables.

In Fig. 3 the results of this numerical study are presented. Fig. 3(a) compared the mean of the minima of the functions, and their 95% CI, found over 100 realisations with the said techniques. As expected, GA_100 generally identified the lowest values. However, as shown in Fig. 3(b), which deals with the number of evaluations to convergence, the price is that many more iterations, two orders of magnitudes more, are needed. The CI is not represented due to its negligible magnitude when compared to the number of evaluations. In terms of precision, rEGO outperformed EGO_EI, GA_10, and GA_100 for the Modified Branin Function, same

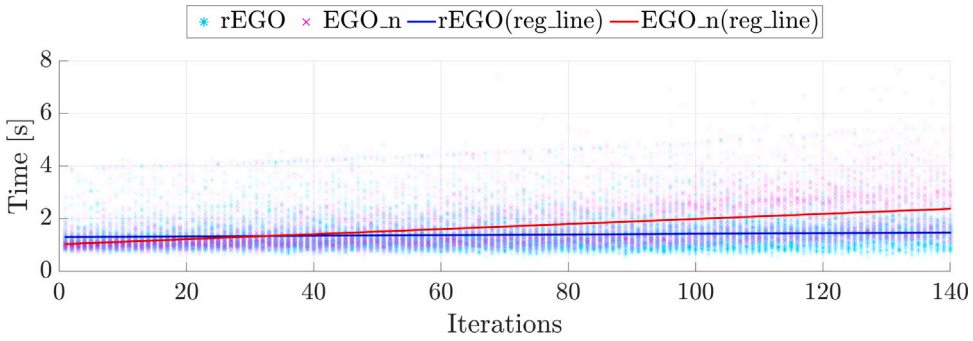

Fig. 4. Elapsed time for each iteration of rEGO and EGO_n for the Styblinkski-Tang function. The scatter represents the actual measurements and solid lines are the regression lines (reg_line).

Table 2
Preliminary study: Potential goal functions for FEMU.

Function	Formula
Residuals of the mean of the MAC diagonal	$1 - \mu(\text{MAC}(\boldsymbol{\phi}_i^E, \boldsymbol{\phi}_i^N))$
Total modal assurance citerion (TMAC) [55]	$1 - \prod_{i=1}^{m} \text{MAC}(\boldsymbol{\phi}_i^E, \boldsymbol{\phi}_i^N)$
Modified total modal assurance criterion (MTMAC) [30]	$1 - \prod_{i=1}^{n} \frac{\text{MAC}(\boldsymbol{\phi}_i^E, \boldsymbol{\phi}_i^N)}{\left(1 + \frac{\lvert\omega_i^N - \omega_i^E\rvert}{\lvert\omega_i^N + \omega_i^E\rvert}\right)}$
Root mean square error (RMSE) of the natural frequencies	$\text{RMSE}(fi_i^E, fi_i^N)$
RMSE of the natural frequencies and mode shapes	$\text{RMSE}(fi_i^E, fi_i^N) + \text{RMSE}(\boldsymbol{\phi}_i^E, \boldsymbol{\phi}_i^N)$

for the Hartman-4D. However, for the Rastrigin function rEGO outperformed all the surrogate-based techniques, but not the two GAs. Finally, for the Styblinkski-Tang function rEGO outperforms EGO_EI, lays in the CI of EGO_n and falls short of the two GAs. Unsurprisingly, the GAs are able to obtain better minimums as they use many more function evaluations when compared to rEGO and EGO. On the other hand, the baseline EGO is less precise for all functions, while the iteration-limited implementation reaches better performance, due to having more function evaluations. This proves that the preliminary study for the ϵ_1 is justified as the baseline EI value of 1% would have brought much worse results. The performance of rEGO and EGO_n are comparable, with the latter, resulting slightly worse for the Modified Branin function and the Rastrigin. rEGO is more computationally efficient.

In Fig. 4 the elapsed time for each iteration of 100 realisations of rEGO and EGO_n for the Styblinkski-Tang function is presented. The scatter represents the time measured for each iteration and the solid lines are the regression lines, respectively rEGO(reg_line) and EGO_n(reg_line) for rEGO and EGO_n. Clearly, the slope of EGO_n(reg_line) is much steeper than its rEGO counterpart. This is only presented for one function as results are similar for any possible function since the speed of the computation depends mainly on the amount of data. This has to do with the way EGO, and Kriging, work. In fact, if refinement and selection are not implemented the data matrix of the model keeps growing and slows down the computation. However, if the refinement and selection are implemented, the computational time remains more stable. Consequently, it can be said that rEGO's computational performance is more efficient than EGO_n. Hence, justifying its implementation.

4. Model updating via rEGO

After having benchmarked rEGO against existing methods, its practical implementation is taken under scrutiny. Within this section, rEGO is used for the FEMU of numerical and experimental systems. However, prior to diving into the FEM application, a suitable goal function needs to be defined. In fact, rEGO clearly works as an optimisation technique and it needs a function to search. Most commonly in FEMU, modal parameters are sought as the driving force of model updating. Hence, a set of five functions are selected for the preliminary study and are shown in Table 2.

The five functions are used to update the FEM of a numerical case study: a 5-element Euler–Bernoulli cantilever beam, as shown in Fig. 5.

The beam is made of Aluminium, resulting in the following properties: Young modulus, E, is 70 GPa and the density, ρ, is 2700 kg/m^{-3}. The beam is 1 m long, L, and its cross-section is a square with 20 mm sides, resulting in a second moment of area, I, of 1.33×10^{-8} mm^4 and an area, A, of 4×10^{-4} mm^2. The beam mass and stiffness matrices are modelled as per theory with vertical displacement and rotation degrees of freedom (DoF). The said properties define the beam's baseline scenario, while a 10% reduction of stiffness in elements 2 and 3 and a 5% reduction of stiffness in elements 4 and 5 characterise the second scenario. For the purpose of this study, the former is known as a baseline and the latter as pseudo-experimental. Table 3 summarises the beam model scenarios and Table 4 shows the first five, for conciseness, natural frequencies of the baseline and pseudo-experimental system.

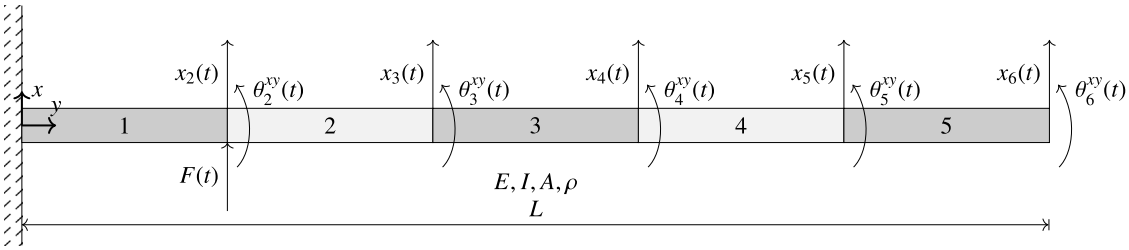

Fig. 5. Preliminary study: 5-element Euler–Bernoulli cantilever beam.

Table 3
Preliminary study: Beam model scenarios.

Scenarios	Description
Baseline	baseline configuration as described above
Pseudo-experimental	10% reduction of stiffness in elements 2 and 3 and a 5% reduction of stiffness in elements 4 and 5

Table 4
Preliminary study: First five natural frequencies of the baseline and pseudo-experimental beam model.

Mode #	Natural frequency [Hz]	
	Baseline	Experimental
1	16.443	16.098
2	103.098	99.928
3	289.570	280.946
4	572.042	553.945
5	949.446	920.842

This example mimics the mismatch between real structures and preliminary FEMs. In order to tune the beam model from the baseline to the pseudo-experimental results, a GA, such as the one previously defined as GA_100, is used in 100 independent realisations, as runs of the FE model updating algorithms. The objective of this analysis is to find the function which offers the best compromise in terms of computational effort, number of evaluations, and precision, which is a two-fold objective as it considers both objective minimisation and parameters evaluation, the latter being critical for SHM applications.

In order to tune the model, a parameter, x_i, is used to scale a beam's element stiffness, k_i^e in such a fashion:

$$k_n^e(x_i) = k_i^e \times x_i \tag{9}$$

The beam stiffness elements are then assembled as usual and the system's modal properties are obtained through eigenanalysis. Hence, the optimisation problem is to minimise the functions in Table 2 by changing the ratios x_i and so tweaking the model's stiffness. The parameters search bound is set between 0.7 and 1.

The results of this study are reported in Fig. 6, where Fig. 6(a) compares the numbers of average evaluations to convergence and the mean values of the minimised objectives ($f(x)$). In Fig. 6(b) the evaluations are compared with the mean euclidean distance between the parameters ($\sqrt[5]{x}$, because the number of variables is five). Only the mean values (μ) are reported as the standard deviation (σ) is found to be of at least two orders of magnitude less than the μ.

Fig. 6(a) shows that the MAC-based functions obtain the smallest $f(x)$ values and the RMSE based ones the highest values. This is somewhat expected as the RMSE-based functions are not scaled between 0 and 1 as the other three. Nevertheless, this outcome is reverted in Fig. 6(b), which shows that the parameters are massively misidentified by the MAC-based goal functions. The best goal function for parameter identification is the MTMAC. In fact, it has better results, both in terms of objective and parameters, than the RMSE techniques for a comparable number of iterations. The MAC-only techniques are discarded because they do not offer a real correlation between the minimised model and the real structure, as shown by the parameters mismatch. Hence, the MTMAC is selected as the objective function for the FEMU via rEGO.

5. Three-storey frame structure

After having established the rEGO theoretical and practical backbone for FEMU, a hybrid, numerical and experimental, case study is selected. The system is a three-storey frame structure, as shown in Fig. 7 developed at the Engineering Institute at LANL [3]. The structure has been widely used as a benchmark for SHM [56–59].

The three-storey frame structure is made of four Aluminium plates (30.5 ×30.5 × 2.5 cm) stacked over four, twelve total, Aluminium columns (17.7 ×2.5 × 0.6 cm) on each floor. The columns connect the adjacent corners of the plate to constitute a frame-like structure. An additional Aluminium column (15.0 × 2.5 × 2.5 cm) hangs from the top plate and it is used to simulate the

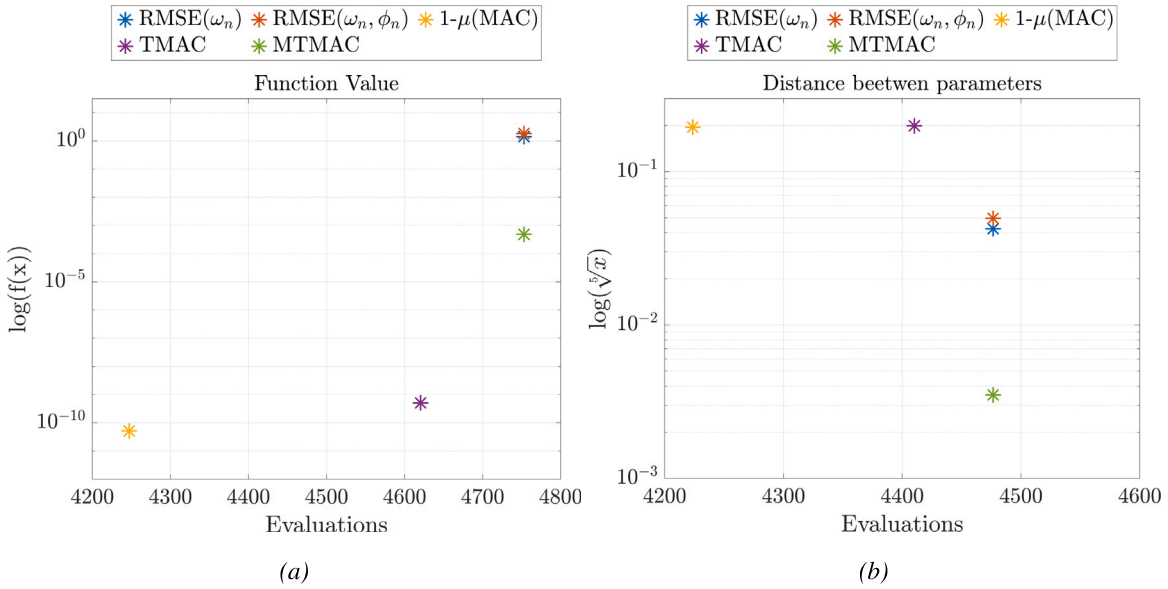

Fig. 6. Preliminary study: Results of the numerical study concerning the goal function selection. Fig. 6(a) shows the average objective over 100 realisations for the five functions, while Fig. 6(b) shows the precision of the estimation of the parameters as the average Euclidean distance between the expected and the computed value.

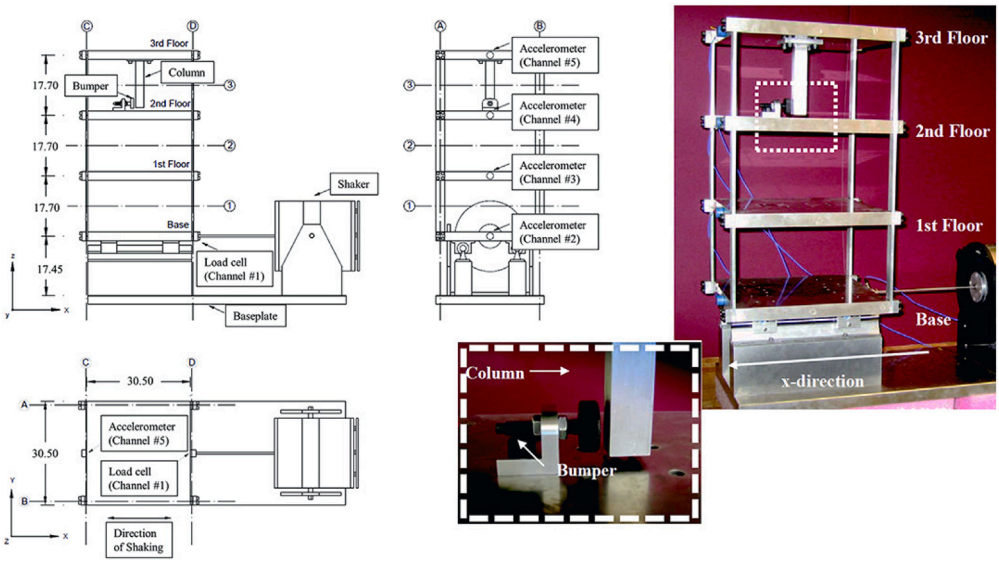

Fig. 7. Three-storey frame structure: Experimental test set-up and schematic diagrams of the three-storey frame structure.
Source: Adapted from [3,60].

nonlinear behaviour induced by its interaction with a bumper placed on the second floor (see the zoomed-in particular in Fig. 7), which can be considered as a breathing crack mechanism [61]. The frame is excited in the transverse direction at the base plate, which is also constrained on rails to allow displacements only in that direction. The data collected refer to four accelerometers, respectively placed at the centreline of each floor and to a load cell attached between the base and the stinger. The accelerometers have a nominal sensitivity of 1000 mVg^{-1} and the load cell of 2.2 mVN^{-1}. The structure is excited with a 2.6 V RMS in the Dactron system, which equals to approximately 20 N RMS measured at the input load cell. The selected excitation signal is a band-limited random excitation between 20 and 150 Hz, where the lower bound is selected to avoid a rigid body mode, and lasting 25.6 s.

The testbed includes 17 independent cases; however, for the scope of this work, only cases # 1–5 are considered. These cases include damage and simulated damage, by the means of mass addition, scenarios. Respectively, case 1, the baseline, represents the

Table 5
Three-storey frame structure: damage and nonlinear scenarios.

Case #	Description
1	Linear, baseline
2	Linear, added mass of 1.2 kg at the base
3	Linear, added mass of 1.2 kg at the first floor
4	Linear, 87.5% stiffness reduction in one column of the first inter-storey
5	Linear, 87.5% stiffness reduction in two columns of the first inter-storey

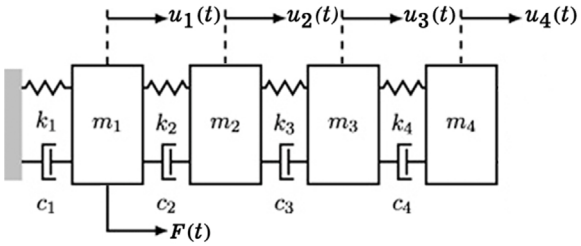

Fig. 8. Three-storey frame structure: equivalent mass–spring–damper system.
Source: Adapted from [62].

system in clean configuration. This is used for the preliminary model updating, as a reference for cases # 2–5, and as a base to build the baseline numerical model for the numerical study. Table 5 summarises the pertinent cases.

Fifty realisations for each case exist, with each instance including time histories recording for the input force, in N, and accelerations, in g. The focus of this work is model updating via modal parameters. Benchmark data for the system under scrutiny is only available in terms of ω_n and ζ_n, since $\boldsymbol{\phi}_n$ values are not quantitatively given in [3]. Hence, ω_n and ζ_n are retrieved from the benchmark data, while $\boldsymbol{\phi}_n$ are retrieved from [62], where they are identified with the Loewner Framework, a modal parameters extraction method introduced by the authors [62–64]. These data are considered as the average over fifty realisations of the same case. The reader interested in a more detailed description of the experimental system is referred to [3].

5.1. Model updating

According to [3], the frame can be represented as a 4 DoF system, with each DoF corresponding to a floor, or plate. These take the form of a classic mass–spring–damper system:

$$\boldsymbol{M}\ddot{\boldsymbol{x}} + \boldsymbol{C}\dot{\boldsymbol{x}} + \boldsymbol{K}\boldsymbol{x} = \boldsymbol{F}(t) \tag{10}$$

where $\boldsymbol{M}$, $\boldsymbol{C}$, and $\boldsymbol{K}$ are respectively the mass, damping, and stiffness matrices, $\boldsymbol{F}(t)$ is the input force vector and $\boldsymbol{x}$ is the displacements vector. $\boldsymbol{M}$ and $\boldsymbol{K}$ are constructed in accordance with standard practice for such systems, while $\boldsymbol{C}$ is built by considering the uncoupled modal damping assumption in [65]:

$$\boldsymbol{C} = \boldsymbol{\phi}^{-T}\boldsymbol{C}_n\boldsymbol{\phi}^{-1} \quad \text{for} \quad \boldsymbol{C}_n = 2\zeta_n\omega_n M_n \tag{11}$$

$\boldsymbol{\phi}$ are the eigenvectors from the eigenanalysis involving $\boldsymbol{M}$ and $\boldsymbol{K}$, $\boldsymbol{C_n}$ is the uncoupled modal damping matrix, ζ_n is the nth damping ratio, ω_n is the nth natural frequency and M_n is the uncoupled modal mass matrix. The mass–spring–damper system equivalent to the three-storey structure is shown in Fig. 8.

$\boldsymbol{M}$ can be assembled considering the structure mass:

$$\boldsymbol{M} = \text{diag}\left\{m_1,\ m_2,\ m_3,\ m_4\right\} \tag{12}$$

where m_n corresponds to the mass of the corresponding floor. Since real mass values are not specified in [3], by assuming the density of Aluminium to be 2700 kgm^{-3} and considering the above-mentioned dimensions for the plates and columns it can be estimated that:

$$\begin{aligned} m_1 &= 6.442 \text{ kg} \\ m_2 = m_3 &= 6.565 \text{ kg} \\ m_4 &= 6.750 \text{ kg} \end{aligned} \tag{13}$$

Also for $\boldsymbol{K}$, no information about the actual stiffness is supplied in [3]. However, given the material properties of Aluminium and the geometric dimensions of the columns the stiffness of a single column, k_c can be derived [66]:

$$k_c = \frac{12\,\text{EI}_{zz}}{h^3} \tag{14}$$

Table 6
Optimisation technique summary.

Optimisation technique	Description
EGO_EI	Standard EGO
EGO_n	Iterations-limited EGO. The limit comes from the average number of iterations for 100 realisations of rEGO
GA_10	GA with 10 generations
GA_100	GA with 100 generations
GA_1000	GA with 1000 generations

Table 7
Three-storey frame structure: Natural frequencies, in Hz, and MAC values between the experimental $\boldsymbol{\phi}_n$ and those derived from the models.

	Natural frequency [Hz]		
Model	Mode # 2 (%)	Mode # 3 (%)	Mode # 4 (%)
Experimental	30.7	54.2	70.7
FEM_model [3]	29.8 (−2.9)	54.0 (−0.4)	71.6 (1.3)
FEM_base	24.852 (−19.050)	45.813 (−15.475)	59.947 (−15.210)
EGO_EI	30.537 (−0.531)	54.132 (−0.125)	71.234 (0.756)
EGO_n	30.639 (−0.198)	54.181 (−0.035)	70.916 (0.306)
GA_10	30.586 (−0.370)	54.165 (−0.064)	71.073 (0.527)
GA_100	30.699 (−0.004)	54.001 (0.002)	70.729 (0.041)
GA_1000	30.700 (−0.002)	54.200 (0.001)	70.718 (0.026)
rEGO	30.696 (−0.012)	54.200 (0)	70.751 (0.072)

	MAC Value [–] wrt Experimental		
Model	Mode # 2	Mode # 3	Mode # 4
FEM_model [3]	NA	NA	NA
FEM_base	0.983	0.999	0.997
EGO_EI	0.991	0.997	0.997
EGO_n	0.990	0.997	0.997
GA_10	0.991	0.997	0.997
GA_100	0.990	0.996	0.996
GA_1000	0.990	0.996	0.996
rEGO	0.990	0.996	0.996

where E is Young's modulus, I_{zz} is the second moment of area of the column, and h is the column height. For this formulation, the discretisation in a mass–spring–damper system means that the stiffness of the equivalent spring is equal to the sum of the columns' stiffness on that floor. Given this information, it is possible to compute the stiffness of the three inter-storey column arrangements: $k_{2-4} = 68.167 \times 10^3$ Nm^{-1}. In accordance with [3], k_1 is modelled to simulate the friction between the rails and the structure and for this use is set to 1 Nm^{-1}, to allow for the large displacements of the rigid body mode outside of the experimental signal bandwith. By the same argument, also ζ_1 is set to zero. For modelling the shear frame structure under scrutiny several implications and simplifications are made. In particular, the axial deformation of columns and the linked axial forces are neglected.

Having defined $\boldsymbol{M}$ and $\boldsymbol{K}$, and using the benchmark values for ζ_{2-4} it is possible to extract the modal parameters of the system via eigenanalysis of Eq. (10) (by setting $\boldsymbol{F}$ to zero). This allows updating the developed model using the benchmark and experimental data described above. The updating is carried out as described for the beam model, with the difference that this time rEGO's performance is going to be compared with EGO_EI, EGO with a number of function evaluations equals to the mean over 100 iterations of rEGO (EGO_n) and three GAs with, respectively, 10 (GA_10), 100 (GA_100), and 1000 (GA_1000) generations. For all scenarios and methods, the FEMU is run 100 times to obtain statistically significant results.The optimisation techniques are summarised in Table 6.

Results of the updating procedures are presented in Table 7. Experimental refers to the data reported in [3] (for ω_n) and those from LF (for $\boldsymbol{\phi}_n$), FEM_model identifies the data, only ω_n is quantitatively available, from the FEM developed in [3], FEM_base indicates the results from the baseline model developed in this section and the others identify the results, obtained from the input parameters average over 100 realisations, for rEGO and the comparative techniques. Also, Table 8 reports the number of required functions evaluations, in terms of mean (to the nearest integer), minimum and maximum over 100 realisations.

The model developed for the frame structure in this section (FEM_base) clearly underestimates ω_{2-4} of the real frame, but it still coherently matches $\boldsymbol{\phi}_{2-4}$. However, a ω_{2-4} relative error exceeding 15% is not acceptable in a FEM model, so tuning is required. This is carried out via rEGO and can be compared with the said comparative techniques' results. The rEGO updated FEM has ω_{2-4} closer to the experimental value than those obtained from EGO_EI, EGO_n and GA_10 models, while GA_100 results are on par with rEGO. Only GA_1000 derived models outperform rEGO in terms of identified ω_n. On the $\boldsymbol{\phi}_n$ side, the identified $\boldsymbol{\phi}_n$ are all very consistent with those from experimental data and their MAC values are at least 0.99, showing almost perfect correlation. The only exception is FEM_base, where the MAC value is slightly lower for $\boldsymbol{\phi}_2$, being 0.983, which however still shows great coherence.

In terms of evaluations, as shown in Table 8, EGO_EI needs the least function evaluations to converge and GA_1000 the most. rEGO, on average, requires 3.3 times the number of iterations than EGO_EI, but the relative difference, between experimental and identified, of ω_{2-4} obtained through rEGO is at least an order of magnitude less than EGO_EI. Hence, rEGO offers performance on par with the more computationally intensive GAs, but requires a number of function evaluations orders of magnitude less than them. On the other hand, it requires more evaluations than EGO_EI, but it offers a more coherent model, particularly in terms of ω_{2-4}.

Table 8
Three-storey frame structure: Functions evaluations needed for convergence for the model updating case. Mean (to the nearest integer), maximum (Max), and minimum (Min) values of 100 realisations are presented.

	Evaluations [–]		
Model	Mean	Max	Min
EGO_EI	128	233	83
EGO_n	427	427	427
GA_10	2110	2110	2110
GA_100	19210	19210	19210
GA_1000	116669	190210	22630
rEGO	427	655	280

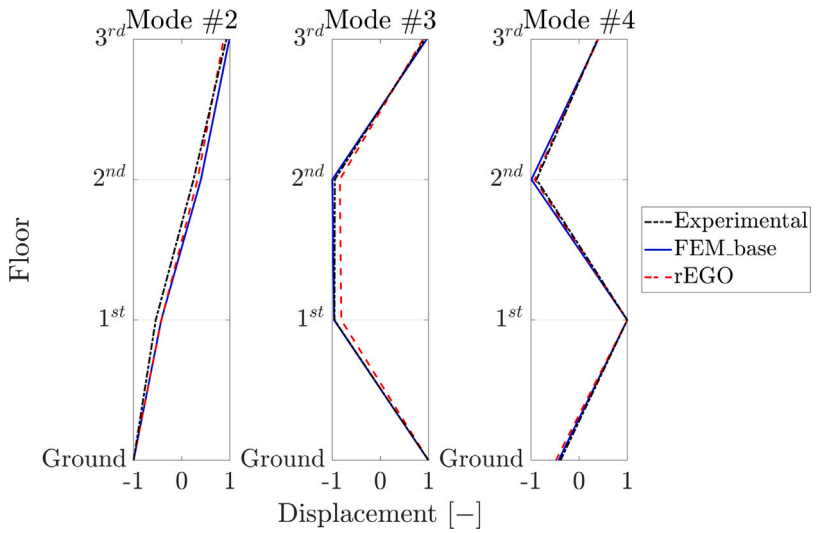

Fig. 9. Three-storey frame structure: Comparison of the $\boldsymbol{\phi}_{2-4}$ identified from Experimental data and computed from FEM_base and rEGO.

For validation purposes, the Experimental, FEM_base, and rEGO $\boldsymbol{\phi}_{2-4}$ are plotted for comparison in Fig. 9.

Notably, the $\boldsymbol{\phi}_{2-4}$ computed from the FEM model have, graphically, a very similar trajectory to those, model-derived, presented in [3].

From now on the FEM updated via rEGO is known as FEM_rEGO and it represents the baseline condition for the numerical and experimental study. The new parameters, in terms of m_n and k_n, of the new model are:

$$m_1 = 6.202 \text{ kg} \quad k_1 = 1 \text{ Nm}^{-1}$$
$$m_2 = 7.504 \text{ kg} \quad k_2 = 398.93 \text{ kNm}^{-1}$$
$$m_3 = 8.225 \text{ kg} \quad k_3 = 464.36 \text{ kNm}^{-1}$$
$$m_4 = 7.656 \text{ kg} \quad k_4 = 457.67 \text{ kNm}^{-1}$$

The differences in mass values between the floors are justified by the fact that the mass of the accessory items is also taken under consideration. These include the columns and the bumper. In fact, the largest mass values are shown for floors 2 and 3 where the hanging column and the bumper are placed.

5.2. Numerical case study

After having successfully updated FEM_base to FEM_rEGO improving the model's fidelity to experimental data, a numerical study is defined. The main goal of the numerical study is to preliminarily assess the capability of rEGO-based model updating to detect damage, modelled as a decrease in stiffness, or by the addition of masses. For these reasons four damage scenarios are postulated: two stiffness reductions and two mass additions. Table 9 defines the damage scenarios characteristics.

The assumption of this approach is that the change in the updated parameters matches the change in the conditions, mass or stiffness, of the structure. This allows the detection of a stiffness decrease and, hence, damage. As previously for the model updating, rEGO is compared with the other methods to assess its precision and performance over 100 realisations, for statistical significance. For the scope of this study ζ_n stay constant for all scenarios, such that $\zeta_{2-4} = [0.06.\ 0.02,\ 0.008]$. In scenarios # 2 and 3 only the stiffness values are updated, giving three variables, while for the remaining two, four masses and three stiffness, are considered

Table 9
Three-storey frame structure: Numerically damaged scenarios.

Scenario #	Description
1	Baseline scenario. Mass and stiffness properties as defined for FEM_rEGO.
2	15% stiffness reduction in the first inter-storey and 10% in the third inter-storey.
3	15% stiffness reduction in the first inter-storey and 20% in the third inter-storey.
4	15% stiffness reduction in the second inter-storey and 10% in the third inter-storey and 2 kg mass addition on the first floor.
5	15% stiffness reduction in the second inter-storey and 20% in the third inter-storey and 2 kg mass addition on the first floor.

Table 10
Three-storey frame structure: Functions evaluations needed for convergence for the numerical case study. Mean (to the nearest integer), maximum (Max), and minimum (Min) values of 100 realisations are presented.

Numerical Case Study - Evaluations [–]												
Scenario	# 2			# 3			# 4			# 5		
Model	Mean	Max	Min	Mean	Max	Min	Mean	Max	Min	Mean	Max	Min
EGO_EI	37	69	32	37	68	32	90	163	75	92	127	76
EGO_n	112	112	112	111	111	111	314	314	314	329	329	329
GA_10	523	523	523	523	523	523	2110	2110	2110	2110	2110	2110
GA_100	4753	4753	4753	4751	4753	4565	19210	19210	19210	19210	19210	19210
GA_1000	13515	34316	5270	12601	32013	4565	66302	190210	22630	69676	176910	22630
rEGO	112	159	60	111	172	67	314	461	172	329	523	188

variables. The search bounds for the stiffness values are [0.7, 1.02] and for the mass values [0.98, 1.3]. Bounds below unity have been selected for stiffnesses as only reductions are expected for damage and similarly, over unity for the masses as only mass addition is foreseen.

The results, in terms of identified change in the parameters, are presented in Fig. 10, where a boxplot is used to condense the results for the 100 realisations. The central mark in the boxes indicates the median, while the bottom and top edges of the box, respectively, indicate the 25th and 75th percentiles. The most extreme data points not considered outliers are comprised within the whiskers. Figs. 10(a) and 10(b), respectively showing the results for scenarios # 2 and 3, only presents the results for the three variables updated, while Figs. 10(c) and 10(d) show results for all the seven variables.

Table 10 shows the required number of function evaluations for convergence for all scenarios and models used within the numerical case study. The results are presented in terms of mean (to the nearest integer), minimum and maximum over 100 realisations.

For all scenarios analysed, Fig. 10 shows that all methods, apart from EGO_EI, give somewhat satisfactory results. However, rEGO outperforms, for nearly all variables in all scenarios and for all comparative methods. In Fig. 10(a), for scenario # 2 the higher generations GA and rEGO perform very similarly, while EGO_n performs slightly worse. EGO_EI and GA_10 are well behind. Nevertheless, all the methods are somewhat consistent such that their median line overlaps, or it is close to overlapping, the numerical damage line. The same can be said for scenario # 3 in Fig. 10(b). Things start to change for the more complex scenarios, # 4 and 5, where also the mass values are considered. In Fig. 10(c), the results for the variable changes for scenario # 4 are presented and rEGO-derived parameters are the most accurate, in terms of median and 23th to 75th percentile. However, for one instance, k_4, rEGO slightly overestimates the stiffness value. EGO_n's median line seems to perfectly match the numerical value, but at the cost of more uncertainty, a bigger box. Hence, rEGO is still the best compromise, precision-wise, even for its least-performing value. An identical occurrence is identified in Fig. 10(d), but the same conclusion can be drawn in favour of rEGO. Notably, the maximum difference from the numerical value for rEGO computed variables never exceeds 1%, for all cases and for both mass and stiffness values.

Concerning the required number of function evaluations for convergence, a similar situation to the one presented in Section 5.1 is found. From Table 10 it is clear that GA_10 and GA_100 struggle to converge before the maximum number of evaluations is reached. This is clear from the fact that the values presented for them are all equal to the maximum values. Once again, EGO_EI requires the least number of evaluations to converge, but, as aforementioned, it is less precise than all methods, and particularly much worse than rEGO. On the other hand, rEGO takes two orders of magnitude fewer evaluations to converge when compared with GA_1000, one to two when compared with GA_100 and at least two-thirds less than GA_10.

Given these results, it can be asserted that rEGO is suitable for the model updating for damage detection in numerical systems, particularly rEGO is able to both damage localisation and severity assessments.

5.3. Experimental case study

After having updated the baseline FEM and verified the feasibility of damage detection on a numerically damaged system, model updating for damage detection via rEGO is tested on the experimental case study from EI at LANL: the three-storey frame structure. As aforementioned, for the sake of model updating, cases # 2–5 from Table 5 are considered. Table 11 shows the characteristics of cases # 1–5 in terms of decrease, or increase, of parameters relative to the updated baseline model in .

Notably, cases # 2–3 deal with a mass addition and # 4–5 with a stiffness reduction in the first inter-storey. There are no experimental cases where mass and stiffness values are changed at the same time. Hence, for cases # 2–3 only the mass values are

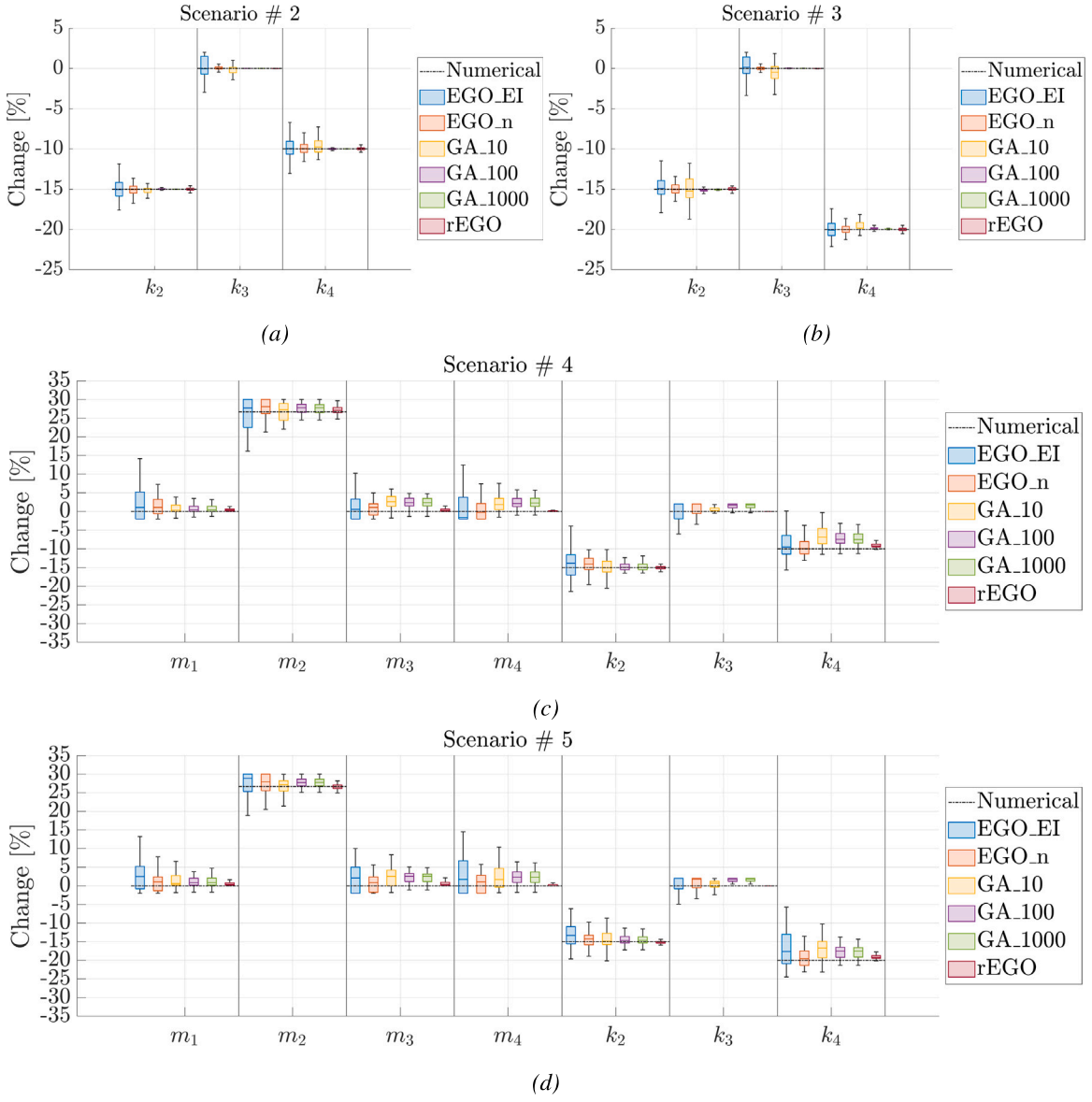

Fig. 10. Three-storey frame structure: Results, in terms of identified change in the parameters, of the numerical study for the four damaged scenarios. Scenario # 2 is shown in Fig. 10(a), Scenario # 3 in Fig. 10(b), Scenario # 4 in Fig. 10(c), and Scenario # 5 in Fig. 10(d).

Table 11
Three-storey frame structure: cases under scrutiny.

Case #	Description
1	Baseline
2	19.35% mass addition at the base
3	15.99% mass addition at the first floor
4	21.88% stiffness reduction in the first inter-storey
5	43.75% stiffness reduction in the first inter-storey

tuned, and, likewise, for cases # 4–5, only the stiffness values are. The procedure is as followed for the previous case study: rEGO and the comparative methods are used to match FEM_rEGO to experimental data for detecting damage, or changes, in the structure via its modal parameters. The procedure is repeated 100 times for each method and case for statistical significance. The search bounds for the mass values are $[0.98,\ 1.5]$ and for the stiffness values are $[0.5,\ 1.02]$.

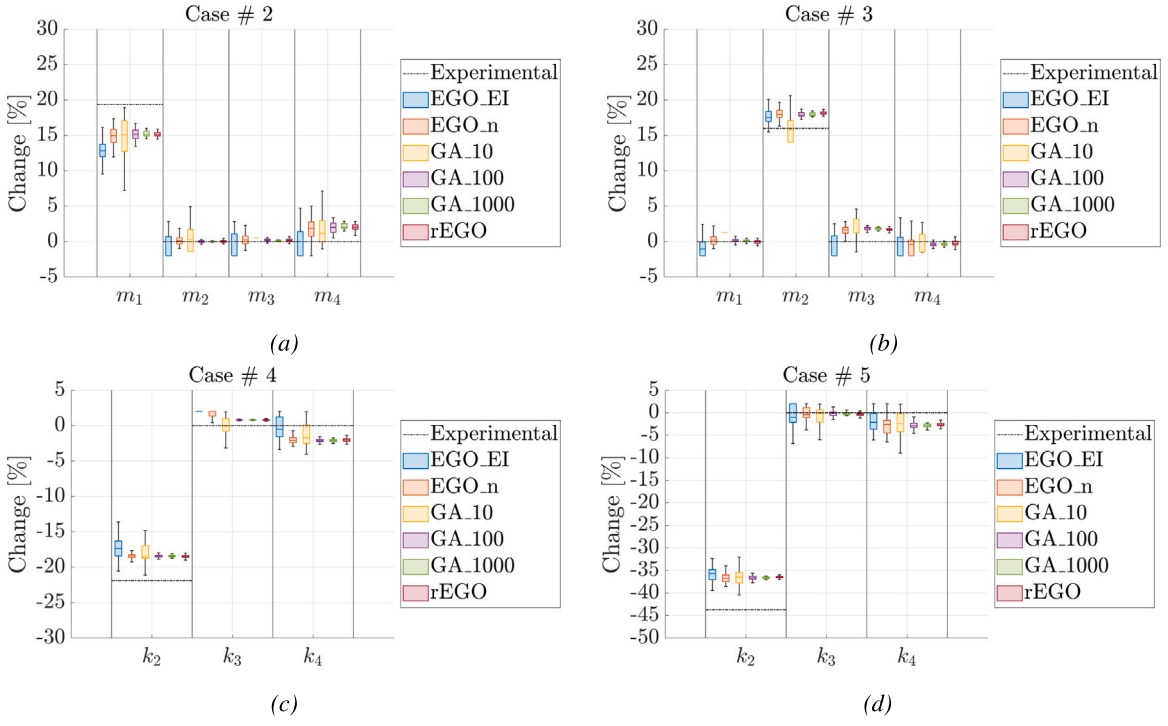

Fig. 11. Three-storey frame structure: Results, in terms of identified change in the parameters, for the experimental case study. Case # 2 is shown in Fig. 11(a), case # 3 in Fig. 11(b), case # 4 in Fig. 11(c), and case # 5 in Fig. 11(d).

In Fig. 11, the results for the changes in parameters are presented in a boxplot, as in the numerical case study, that allows understanding the stability, as in the 25th and 75th percentiles, and precision, median value, of each method.

For case #2 (Fig. 11(a)) m_2 amd m_3 are well identified by all methods apart EGO_EI and GA_10, particularly for m_2. On the other hand, m_4 is slightly overestimated by the more precise methods, GA_1000 and rEGO, and unstable results, in terms of 25th and 75th percentiles, are reported for the remaining. However, all methods clearly identify a prominent mass change in the base floor with rEGO and GA_1000 showing the best compromise between stability and precision. In fact, GA_10 upper whisker is closer to the expected value, but its lower bound falls much lower, between 5 and 10% when the expected value is 19.35%. A similar situation can be seen for case # 3 in Fig. 11(b), where, however, the slightly overestimated masses is m_3 and m_2, the increased mass, is actually overestimated rather than underestimated. Notably, the absolute maximum difference between the rEGO-identified parameters and the actual values never exceeds 4.3% for the mass values of case # 2 and 2.2% for those of case # 3.

Cases # 4 and 5 deal with the damage, by stiffness reduction, cases. In Fig. 11(c) the results for the computed parameters of k_{2-4} are reported. In case # 4 the damage is localised in the first inter-storey for a stiffness reduction of 21.88% over FEM_rEGO. Damage is successfully localised, but its severity is slightly underestimated, at k_2, by all methods; however, rEGO is the best performing in terms of precision and stability. The maximum absolute difference between the computed and the expected value is 3.4% and it is located in the damaged inter-storey. For the remaining stiffness values, k_3 is slightly overestimated ($< 1\%$) and k_4 is underestimated (2%). A similar situation is found for case # 5, where the damage located in the first inter-storey is modelled with a stiffness reduction of 43.75%. Again, the damage is localised accordingly, but it is underestimated (7.2%). On the other hand, k_3 is perfectly identified and k_4, once again, is underestimated (2.6%).

In terms of computational performance, rEGO, as per other cases, takes many fewer function evaluations, e.g. 2 orders of magnitude less than GA_1000, for convergence. The only method taking fewer function evaluations for convergence is EGO_EI, but at the price of precision. These results are presented in Table 12.

rEGO outperforms all other methods in terms of stability, precision and computational performance. However, all methods seem to be influenced by some bias resulting in over-, or under-, estimation of some values. Since damage is correctly localised and severity reasonably assessed, these differences are to be traced back to the assumptions made in Section 5.1 to characterise the three-storey frame structure with the mass–spring–damper model and to the system's intrinsic nature. Such as in [67], where this phenomenon was more intense and even the localisation of the damage was not feasible using only modal data.

6. High aspect ratio wing spar

In order to further validate the capability of rEGO for damage detection, a numerical case study of a high aspect ratio wing spar is created. The spar's design is inspired by that of the eXperimental Beards 2 wing [68,69] from the Beam Reduction Dynamic

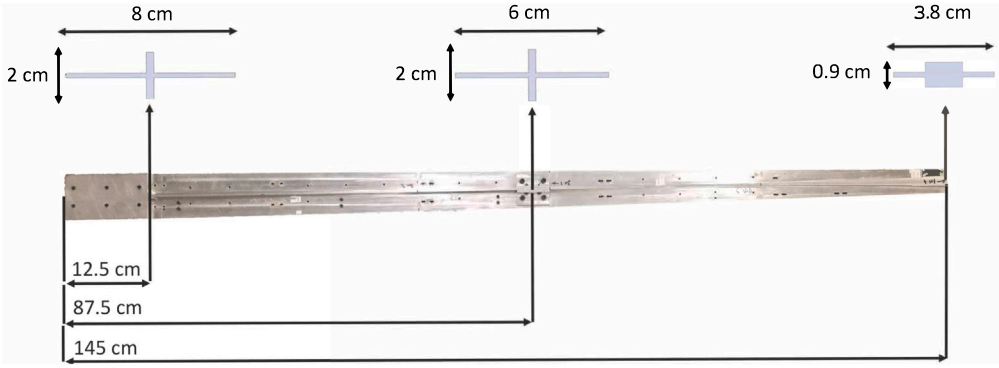

Fig. 12. Top view of the spar with its characterising cross sections. Not in scale.

Table 12
Three-storey frame structure: Functions evaluations needed for convergence for the experimental case study. Mean (to the nearest integer), maximum (Max), and minimum (Min) values of 100 realisations are presented.

Experimental Case Study - Evaluations [–]												
Case #	2			3			4			5		
Model	Mean	Max	Min	Mean	Max	Min	Mean	Max	Min	Mean	Max	Min
EGO_EI	46	51	44	46	54	43	36	42	33	37	49	33
EGO_n	185	185	185	174	174	174	133	133	133	132	132	132
GA_10	523	523	523	523	523	523	523	523	523	523	523	523
GA_100	4753	4753	4753	4753	4753	4753	4725	4753	4142	4746	4753	4048
GA_1000	28952	47053	5646	12727	39110	4753	8865	27689	4142	23938	47053	4048
rEGO	185	247	131	174	277	105	133	195	88	132	204	84

Table 13
Modal parameters of the baseline, target and updated models.

Natural Frequencies [Hz]								
Mode #	1	2	3	5	6	7	9	10
Baseline	5.527	27.267	33.447	90.298	148.556	173.979	278.173	319.738
Target	2.695	13.222	30.679	74.429	133.143	142.319	235.864	301.311
Updated	2.695	13.222	30.669	74.430	133.356	142.143	236.363	301.472
	(0%)	(0%)	(−0.03%)	(0%)	(0.16%)	(−0.12%)	(0.21%)	(0.05%)
MAC Value wrt baseline [–]								
Mode #	1	2	3	5	6	7	9	10
Target	1	1	0.99	0.80	0	0	0.75	0.01
Updated	1	1	0.99	0.80	0	0	0.75	0.01

Scaling project at Cranfield University [70,71]. The geometry of the spar is shown in Fig. 12 and be summarised as a tapered beam, varying linearly according to three characterising cross sections.

A FEM model is built in ANSYS Mechanical APDL using 1450 BEAM188 elements, a rectangular section for the root, and two taper sections, as per Fig. 12. The material is aluminium with Young's modulus, E, of 70 GPa and density, ρ, of 2700 kgm^{-3}. A damage and loaded scenario is introduced for the verification of rEGO capabilities. The scenario includes a reduction of stiffness, modelled as a change in $I_{xx}^{(1-3)}$ and $I_{yy}^{(1-3)}$ of the characterising sections, and a mass addition modelled as lump mass on the cantilever beam. These account for a total of eight parameters (x_n), six concerning the second moments of area and two the mass. In particular, both the mass values and their spanwise position are characterised by the two mass parameters. The optimisation search bound for the parameters relating to the second moments of area is [0.7 1.1] and [0.5 1] for the two related to the added mass. Before starting the FEMU procedure the baseline beam is defined without any damage or mass addition and the modes that show predominantly horizontal and vertical displacements are selected within the first 10 modes. This means that the ω_n and $\boldsymbol{\phi}_n$ of modes # 1, 2, 3, 5, 6, 7, 9, and 10 are considered in computing the MTMAC within the algorithm. In order to collect the displacement data of the $\boldsymbol{\phi}_n$, 20 evenly spaced query positions are selected along the cantilever spar.

After 3173 model evaluations, rEGO returns a minimum MTMAC of 0.003. Tables 13 and 14 show the results of the FEMU procedure and compare it with the expected and baseline values. The values in brackets represent the relative difference, in percentage, between the target and updated values.

Table 14
Parameters values of the baseline, target and updated models.

Model properties								
x_n #	$I_{xx}^{(1)}$ [m^4]	$I_{yy}^{(1)}$ [m^4]	$I_{xx}^{(2)}$ [m^4]	$I_{yy}^{(2)}$ [m^4]	$I_{xx}^{(3)}$ [m^4]	$I_{yy}^{(3)}$ [m^4]	Position [m]	Mass [kg]
Baseline	64895×10^{-12}	2313×10^{-12}	34612×10^{-12}	1904×10^{-12}	12878×10^{-12}	1241×10^{-12}	NA	NA
Target	51916×10^{-12}	2082×10^{-12}	34612×10^{-12}	1523×10^{-12}	10302×10^{-12}	1241×10^{-12}	1.2	0.8
Updated	52800×10^{-12} (1.70%)	2113×10^{-12} (1.52%)	33903×10^{-12} (−2.05%)	1499×10^{-12} (−1.61%)	11262×10^{-12} (9.32%)	1287×10^{-12} (3.68%)	1.199 (−0.11%)	0.808 (1%)
Updating parameters [–]								
Mode #	1	2	3	5	6	7	9	10
Target	0.8	0.9	1	0.8	0.8	1	0.8113	0.8
Updated	0.814	0.914	0.980	0.787	0.875	1.037	0.8105	0.808

In Table 13, the modal parameters are found to be very coherent between the target and updated model. In particular, the difference between the ω_n of the two models is always less than 0.3% and the MAC value with respect to the baseline model are very similar. It can be said that the rEGO updated model is able to mimic the modal behaviour of the target model.

Table 14 shows the parameters applied to the model to determine the updated model and the resulting values. $I_{xx}^{(3)}$ aside, all parameters are very much coherent (less than 4% difference) with the target model. In particular, the mass position and value are correctly identified. This is deemed to be the most challenging part of this procedure as its position or value might have been absorbed by other parameters. However, it must be noted that the reduction in $I_{xx}^{(3)}$ is underestimated by 9.32%; nevertheless, a reduction is still identified in the model.

Yielding the great results of the modal data comparison between the target and updated model and the ability to localise and quantify the added mass, the rEGO is deemed as a suitable alternative for the detection of changes, stiffness or mass related, in a large FEM model.

7. Conclusions

In this work, a computationally efficient version of the well-known Efficient Global Optimization method is proposed. The optimisation technique is named rEGO, refined Efficient Global Optimisation, and it extends the global capability of the original method to a global–local, or hybrid, search. This is achieved with the introduction of a refinement and selection technique, implemented in two steps: search domain reduction and sample points de-clustering. The capability and performance of the new method are tested successfully on four test functions, where the method outperforms its predecessor and performs accordingly to genetic algorithms, in terms of precision, but shows a lower computational burden. This successful implementation is then followed by the introduction of a model updating technique based on rEGO. The technique uses modal parameters, extracted from experimental data, to tune a finite element model via a penalty function, the modified total modal assurance criterion. After validation on a numerical system, a five degrees of freedom cantilever beam, the technique is employed on a well-known experimental dataset from the Engineering Institute at the Los Alamos National Laboratory: the three-storey frame structure. First, a baseline model is developed, and then it is tuned to the real experimental case. The tuned model is then numerically damaged, by stiffness reduction in four cases, two considering damage-only and the other damage and mass addition. Then, rEGO is implemented in four experimental cases for the detection of damage, or mass addition. rEGO is able to detect, localise and quantify damage and mass addition satisfactorily in all cases, numerical and experimental, examined. Finally, rEGo is successfully implemented on a finite element model of a wing spar built in ANSYS Mechanical APDL for the identification of changes in stiffness and mass on the structure. For these reasons, the authors highly recommend the use of model updating via rEGO for the detection of damage in mechanical and civil structures and the implementation of rEGO as a single-objective optimisation technique over existing ones, such as very computationally heavy genetic algorithms. Also, the authors' implementation of rEGO is made available in an open repository.

CRediT authorship contribution statement

Gabriele Dessena: Conceptualization, Methodology, Software, Validation, Formal analysis, Investigation, Data curation, writing – original draft, Writing – review & editing, Visualization. **Dmitry I. Ignatyev:** Resources, Writing – review & editing, Visualization, Supervision . **James F. Whidborne:** Resources, Writing – review & editing, Visualization, Supervision. **Luca Zanotti Fragonara:** Resources, Writing – review & editing, Supervision, Funding acquisition.

Declaration of competing interest

The authors declare that they have no known competing financial interests or personal relationships that could have appeared to influence the work reported in this paper.

Data availability

The experimental data that support the findings of this study are available in the Engineering Institute at Los Alamos National Laboratory website at https://www.lanl.gov/projects/national-security-education-center/engineering/ei-software-download/index.php (Data file 1) and more data that supports this study (Data file 2) can be accessed through the Cranfield University repository (CORD) at https://doi.org/10.5281/zenodo.8406030.

This project contains the following underlying data:

Data file 1. The three-storey structure dataset from the Engineering Institute at Los Alamos National Laboratory

Data file 2. A tutorial on the rEGO for model updating

Data file 2 is available under the terms of the [GNU General Public License v3.0 (GPL 3.0)].

Acknowledgements

The authors would like to thank the Engineering Institute at Los Alamos National Laboratory for providing the experimental data used in this article.

Funding

The authors disclosed receipt of the following financial support for the research, authorship, and/or publication of this article: This work was supported by the Engineering and Physical Sciences Research Council (EPSRC), UK [grant number 2277626].

References

[1] D.R. Jones, M. Schonlau, W.J. Welch, Efficient global optimization of expensive black-box functions, J. Global Optim. 13 (1998) 455–492, http://dx.doi.org/10.1023/A:1008306431147.

[2] D.G. Krige, A statistical approach to some basic mine valuation problems on the Witwatersrand, J. Chem. Metallurg. Min. Soc. South Afr. 52 (6) (1951) 119–139.

[3] E. Figueiredo, G. Park, J. Figueiras, C. Farrar, K. Worden, Structural Health Monitoring Algorithm Comparisons Using Standard Data Sets. Vol. LA-14393, Tech. Rep., Los Alamos National Laboratory (LANL), Los Alamos, NM (United States), 2009, http://dx.doi.org/10.2172/961604, URL http://www.osti.gov/servlets/purl/961604-nweA8p/.

[4] P. Ni, J. Li, H. Hao, Q. Han, X. Du, Probabilistic model updating via variational Bayesian inference and adaptive Gaussian process modeling, Comput. Methods Appl. Mech. Engrg. 383 (2021) 113915, http://dx.doi.org/10.1016/j.cma.2021.113915, https://linkinghub.elsevier.com/retrieve/pii/S0045782521002528.

[5] H. Moravej, S. Jamali, T.H. Chan, A. Nguyen, Finite element model updating of civil engineering infrastructures: A literature review, in: SHMII 2017 - 8th International Conference on Structural Health Monitoring of Intelligient Infrastructure, Proceedings, 2017, pp. 1139–1150.

[6] J.E. Mottershead, M.I. Friswell, Model updating in structural dynamics: A survey, J. Sound Vib. 167 (2) (1993) 347–375, http://dx.doi.org/10.1006/jsvi.1993.1340.

[7] W.-X. Ren, H.-B. Chen, Finite element model updating in structural dynamics by using the response surface method, Eng. Struct. 32 (8) (2010) 2455–2465, http://dx.doi.org/10.1016/j.engstruct.2010.04.019.

[8] L. Zanotti Fragonara, G. Boscato, R. Ceravolo, S. Russo, S. Ientile, M.L. Pecorelli, A. Quattrone, Dynamic investigation on the Mirandola bell tower in post-earthquake scenarios, Bull. Earthq. Eng. 15 (1) (2017) 313–337, http://dx.doi.org/10.1007/s10518-016-9970-z.

[9] M. Girardi, C. Padovani, D. Pellegrini, M. Porcelli, L. Robol, Finite element model updating for structural applications, J. Comput. Appl. Math. 370 (2020) 112675, http://dx.doi.org/10.1016/j.cam.2019.112675, arXiv:1801.09122.

[10] C.J. Stull, C.J. Earls, P.-S. Koutsourelakis, Model-based structural health monitoring of naval ship hulls, Comput. Methods Appl. Mech. Engrg. 200 (9–12) (2011) 1137–1149, http://dx.doi.org/10.1016/j.cma.2010.11.018, https://linkinghub.elsevier.com/retrieve/pii/S0045782510003427.

[11] C.R. Farrar, S.W. Doebling, D.A. Nix, Vibration–based structural damage identification, in: N.A.J. Lieven, D.J. Ewins (Eds.), Phil. Trans. R. Soc. A 359 (1778) (2001) 131–149, http://dx.doi.org/10.1098/rsta.2000.0717, URL https://royalsocietypublishing.org/doi/10.1098/rsta.2000.0717.

[12] P. Cawley, Structural health monitoring: Closing the gap between research and industrial deployment, Struct. Health Monit. 17 (5) (2018) 1225–1244, http://dx.doi.org/10.1177/1475921717750047.

[13] M. Civera, G. Calamai, L. Zanotti Fragonara, System identification via fast relaxed vector fitting for the structural health monitoring of masonry bridges, Structures 30 (January) (2021) 277–293, http://dx.doi.org/10.1016/j.istruc.2020.12.073.

[14] J. Zacharias, C. Hartmann, A. Delgado, Damage detection on crates of beverages by artificial neural networks trained with finite-element data, Comput. Methods Appl. Mech. Engrg. 193 (6–8) (2004) 561–574, http://dx.doi.org/10.1016/j.cma.2003.10.009.

[15] N.F. Alkayem, M. Cao, Y. Zhang, M. Bayat, Z. Su, Structural damage detection using finite element model updating with evolutionary algorithms: A survey, Neural Comput. Appl. 30 (2) (2018) 389–411, http://dx.doi.org/10.1007/s00521-017-3284-1.

[16] H. Sohn, C.R. Farrar, F. Hemez, J. Czarnecki, D.D. Shunk, D.W. Stinemates, B.R. Nadler, J. Czarnecki, A Review of Structural Health Monitoring Literature: 1996–2001, Tech. rep., Los Alamos National Laboratory (LANL), Los Alamos, CA, 2004, pp. 1–7, URL https://www.osti.gov/servlets/purl/976152.

[17] M. Baruch, Optimization procedure to correct stiffness and flexibility matrices using vibration tests, AIAA J. 16 (11) (1978) 1208–1210, http://dx.doi.org/10.2514/3.61032, URL https://arc.aiaa.org/doi/10.2514/3.61032.

[18] R.G.J. Ross, Synthesis of stiffness and mass matrices from experimental vibration modes, SAE Trans. 80 (4) (1971) 2627–2635, URL https://www.jstor.org/stable/44650348.

[19] J. Sidhu, D.J. Ewins, Correlation of finite element and modal test studies of a practical structure, in: Proceedings of the 2nd IMAC, Orlando, FL, 1984, pp. 756–762.

[20] D.C. Zimmerman, M. Kaouk, Eigenstructure assignment approach for structural damage detection, AIAA J. 30 (7) (1992) 1848–1855, http://dx.doi.org/10.2514/3.11146, URL https://arc.aiaa.org/doi/10.2514/3.11146.

[21] Z. Wang, R. Lin, M. Lim, Structural damage detection using measured FRF data, Comput. Methods Appl. Mech. Engrg. 147 (1–2) (1997) 187–197, http://dx.doi.org/10.1016/S0045-7825(97)00013-3, URL https://linkinghub.elsevier.com/retrieve/pii/S0045782597000133.

[22] A. Teughels, G. De Roeck, Damage detection and parameter identification by finite element model updating, Arch. Comput. Methods Eng. 12 (2) (2005) 123–164, http://dx.doi.org/10.1007/BF03044517, URL http://link.springer.com/10.1007/BF03044517.

[23] G. Boscato, S. Russo, R. Ceravolo, L.Z. Fragonara, Global sensitivity-based model updating for heritage structures, Comput.-Aided Civ. Infrastruct. Eng. 30 (8) (2015) 620–635, http://dx.doi.org/10.1111/mice.12138, URL https://onlinelibrary.wiley.com/doi/10.1111/mice.12138.
[24] T. Marwala, Finite-Element-Model Updating using Computional Intelligence Techniques, Springer, London, 2010, http://dx.doi.org/10.1007/978-1-84996-323-7.
[25] T. Marwala, S. Sibisi, Finite element model updating using bayesian framework and modal properties, J. Aircr. 42 (1) (2005) 275–278, http://dx.doi.org/10.2514/1.11841, URL https://arc.aiaa.org/doi/10.2514/1.11841.
[26] R. Rocchetta, M. Broggi, Q. Huchet, E. Patelli, On-line Bayesian model updating for structural health monitoring, Mech. Syst. Signal Process. 103 (2018) 174–195, http://dx.doi.org/10.1016/j.ymssp.2017.10.015.
[27] A. Keane, J. Scanlan, Design search and optimization in aerospace engineering, Phil. Trans. R. Soc. A 365 (1859) (2007) 2501–2529, http://dx.doi.org/10.1098/rsta.2007.2019, URL https://royalsocietypublishing.org/doi/10.1098/rsta.2007.2019.
[28] D.E. Goldberg, Genetic Algorithms in Search, Optimization and Machine Learning, Addison-Wesley Longman, Boston, MA, 1989, p. 372.
[29] X. Yang, X. Guo, H. Ouyang, D. Li, A Kriging model based finite element model updating method for damage detection, Appl. Sci. 7 (10) (2017) 1039, http://dx.doi.org/10.3390/app7101039.
[30] R. Perera, R. Torres, Structural damage detection via modal data with genetic algorithms, J. Struct. Eng. 132 (9) (2006) 1491–1501, http://dx.doi.org/10.1061/(ASCE)0733-9445(2006)132:9(1491).
[31] M.I. Friswell, J.E. Mottershead, Finite Element Model Updating in Structural Dynamics, in: Solid Mechanics and its Applications, vol. 38, Springer Netherlands, Dordrecht, 1995, http://dx.doi.org/10.1007/978-94-015-8508-8, URL http://link.springer.com/10.1007/978-94-015-8508-8.
[32] A.I.J. Forrester, A. Sóbester, A.J. Keane, Engineering Design via Surrogate Modelling, Wiley, 2008, http://dx.doi.org/10.1002/9780470770801.
[33] A. Sóbester, A.I. Forrester, D.J. Toal, E. Tresidder, S. Tucker, Engineering design applications of surrogate-assisted optimization techniques, Opt. Eng. 15 (1) (2014) 243–265, http://dx.doi.org/10.1007/s11081-012-9199-x.
[34] J. Wang, C. Wang, Structural model updating of frequency response function based on Kriging model, in: 2016 3rd International Conference on Information Science and Control Engineering, ICISCE, IEEE, 2016, pp. 640–644, http://dx.doi.org/10.1109/ICISCE.2016.142, URL http://ieeexplore.ieee.org/document/7726239/.
[35] J. Wang, C. Wang, J. Zhao, Structural dynamic model updating based on kriging model using frequency response data, J. Vibroeng. 18 (6) (2016) 3484–3498, http://dx.doi.org/10.21595/jve.2016.16973.
[36] H. Yin, J. Ma, K. Dong, Z. Peng, P. Cui, C. Yang, Model updating method based on Kriging model for structural dynamics, Shock Vib. 2019 (2019) 1–12, http://dx.doi.org/10.1155/2019/8086024, URL https://www.hindawi.com/journals/sv/2019/8086024/.
[37] G.E.P. Box, K.B. Wilson, On the experimental attainment of optimum conditions, J. R. Stat. Soc. Ser. B Stat. Methodol. 13 (1) (1951) 1–45, URL http://www.jstor.org/stable/2983966.
[38] M.D. McKay, R.J. Beckman, W.J. Conover, A comparison of three methods for selecting values of input variables in the analysis of output from a computer code, Technometrics 21 (2) (1979) 239, http://dx.doi.org/10.2307/1268522.
[39] M.D. Morris, T.J. Mitchell, Exploratory designs for computational experiments, J. Statist. Plann. Inference 43 (3) (1995) 381–402, http://dx.doi.org/10.1016/0378-3758(94)00035-T.
[40] A.I.J. Forrester, A. Sóbester, A.J. Keane, Multi-fidelity optimization via surrogate modelling, Proc. R. Soc. A Math. Phys. Eng. Sci. 463 (2088) (2007) 3251–3269, http://dx.doi.org/10.1098/rspa.2007.1900.
[41] A. Lye, A. Cicirello, E. Patelli, Sampling methods for solving Bayesian model updating problems: A tutorial, Mech. Syst. Signal Process. 159 (2021) 107760, http://dx.doi.org/10.1016/j.ymssp.2021.107760.
[42] A. Sóbester, A.I.J. Forrester, Aircraft Aerodynamic Design: Geometry and Optimization, Wiley, 2014, p. 264.
[43] G. Dessena, D.I. Ignatyev, J.F. Whidborne, L. Zanotti Fragonara, A Kriging approach to model updating for damage detection, in: P. Rizzo, A. Milazzo (Eds.), EWSHM 2022, LNCE 254, Springer, Singapore, 2023, pp. 245–255, http://dx.doi.org/10.1007/978-3-031-07258-1_26, URL https://link.springer.com/10.1007/978-3-031-07258-1{_}26.
[44] J. Xing, Y. Luo, Z. Gao, A global optimization strategy based on the Kriging surrogate model and parallel computing, Struct. Multidiscip. Optim. 62 (1) (2020) 405–417, http://dx.doi.org/10.1007/s00158-020-02495-6.
[45] D. Whitley, A genetic algorithm tutorial, Stat. Comput. 4 (2) (1994) http://dx.doi.org/10.1007/BF00175354, URL http://link.springer.com/10.1007/BF00175354.
[46] I. Voutchkov, A. Keane, Multi-objective optimization using surrogates, in: Y. Tenne, C.-K. Goh (Eds.), Computational Intelligence in Optimization, Springer, Berlin, 2010, pp. 155–175, http://dx.doi.org/10.1007/978-3-642-12775-5_7, URL http://link.springer.com/10.1007/978-3-642-12775-5{_}7.
[47] K. Deb, A. Pratap, S. Agarwal, T. Meyarivan, A fast and elitist multiobjective genetic algorithm: NSGA-II, IEEE Trans. Evol. Comput. 6 (2) (2002) 182–197, http://dx.doi.org/10.1109/4235.996017.
[48] H.B. Nielsen, S.N. Lophaven, J. Søndergaard, DACE - A MATLAB Kriging Toolbox, Tech. rep., Informatics and Mathematical Modelling, Technical University of Denmark, DTU, 2002, URL https://orbit.dtu.dk/en/publications/dace-a-matlab-kriging-toolbox.
[49] D. Zhan, The standard and parallel efficient global optimization (EGO) algorithms, 2017, URL https://github.com/zhandawei/Single{_}objective{_}EGO{_}algorithms.
[50] J. Qian, Y. Cheng, J. Zhang, J. Liu, D. Zhan, A parallel constrained efficient global optimization algorithm for expensive constrained optimization problems, Eng. Optim. 53 (2) (2021) 300–320, http://dx.doi.org/10.1080/0305215X.2020.1722118.
[51] S. Surjanovic, D. Bingham, Virtual library of simulation experiments: Test functions and dataset, 2013, URL http://www.sfu.ca/{~}ssurjano/optimization.html.
[52] V. Picheny, T. Wagner, D. Ginsbourger, A benchmark of Kriging-based infill criteria for noisy optimization, Struct. Multidiscip. Optim. 48 (3) (2013) 607–626, http://dx.doi.org/10.1007/s00158-013-0919-4.
[53] L. Rastrigin, Systems of External Control, Mir, Moscow, 1974.
[54] M. Jamil, X.S. Yang, A literature survey of benchmark functions for global optimisation problems, Int. J. Math. Model. Numer. Optim. 4 (2) (2013) 150, http://dx.doi.org/10.1504/IJMMNO.2013.055204, URL http://www.inderscience.com/link.php?id=55204.
[55] Y. Gao, B.F. Spencer, Damage localization under ambient vibration using changes in flexibility, Earthq. Eng. Eng. Vibr. 1 (1) (2002) 136–144, http://dx.doi.org/10.1007/s11803-002-0017-x, URL http://link.springer.com/10.1007/s11803-002-0017-x.
[56] M. Civera, M. Ferraris, R. Ceravolo, C. Surace, R. Betti, The Teager-Kaiser energy cepstral coefficients as an effective structural health monitoring tool, Appl. Sci. 9 (23) (2019) 5064, http://dx.doi.org/10.3390/app9235064, URL https://www.mdpi.com/2076-3417/9/23/5064.
[57] D. Martucci, M. Civera, C. Surace, The extreme function theory for damage detection: An application to civil and aerospace structures, Appl. Sci. 11 (4) (2021) 1716, http://dx.doi.org/10.3390/app11041716, URL https://www.mdpi.com/2076-3417/11/4/1716.
[58] M. Civera, C. Surace, A comparative analysis of signal decomposition techniques for structural health monitoring on an experimental benchmark, Sensors 21 (5) (2021) 1825, http://dx.doi.org/10.3390/s21051825, URL https://www.mdpi.com/1424-8220/21/5/1825.
[59] M. Civera, C. Surace, Instantaneous spectral entropy: An application for the online monitoring of multi-storey frame structures, Buildings 12 (3) (2022) 310, http://dx.doi.org/10.3390/buildings12030310, URL https://www.mdpi.com/2075-5309/12/3/310.
[60] M. Civera, G. Calamai, L. Zanotti Fragonara, Experimental modal analysis of structural systems by using the fast relaxed vector fitting method, Struct. Control Health Monit. 28 (4) (2021) 1–23, http://dx.doi.org/10.1002/stc.2695.

[61] A. Bovsunovsky, C. Surace, Non-linearities in the vibrations of elastic structures with a closing crack: A state of the art review, Mech. Syst. Signal Process. 62–63 (2015) 129–148, http://dx.doi.org/10.1016/j.ymssp.2015.01.021.

[62] G. Dessena, M. Civera, L. Zanotti Fragonara, D.I. Ignatyev, J.F. Whidborne, A Loewner-Based system identification and structural health monitoring approach for mechanical systems, in: L. Chen (Ed.), Struct. Control Health Monit. 2023 (2023) 1–22, http://dx.doi.org/10.1155/2023/1891062, URL https://www.hindawi.com/journals/schm/2023/1891062/.

[63] G. Dessena, M. Civera, D.I. Ignatyev, J.F. Whidborne, L. Zanotti Fragonara, B. Chiaia, The accuracy and computational efficiency of the loewner framework for the system identification of mechanical systems, Aerospace 10 (6) (2023) 571, http://dx.doi.org/10.3390/aerospace10060571, URL https://www.mdpi.com/2226-4310/10/6/571.

[64] G. Dessena, M. Civera, A. Pontillo, D.I. Ignatyev, J.F. Whidborne, L. Zanotti Fragonara, Novel modal parameters extraction methods for aeronautical structures, 2023, [Submitted to] AIAA Journal.

[65] F. Naeim, J.M. Kelly, Design of Seismic Isolated Structures, John Wiley, Hoboken, NJ, USA, 1999, p. 304, http://dx.doi.org/10.1002/9780470172742, URL http://doi.wiley.com/10.1002/9780470172742.

[66] E.L. Wilson, J. Penzien, Evaluation of orthogonal damping matrices, Internat. J. Numer. Methods Engrg. 4 (1) (1972) 5–10, http://dx.doi.org/10.1002/nme.1620040103, URL https://onlinelibrary.wiley.com/doi/10.1002/nme.1620040103.

[67] F.M. Hemez, S.W. Doebling, Review and assessment of model updating for non-linear, transient dynamics, Mech. Syst. Signal Process. 15 (1) (2001) 45–74, http://dx.doi.org/10.1006/mssp.2000.1351, URL https://linkinghub.elsevier.com/retrieve/pii/S0888327000913517.

[68] G. Dessena, D.I. Ignatyev, J.F. Whidborne, A. Pontillo, L. Zanotti Fragonara, Ground vibration testing of a flexible wing: A benchmark and case study, Aerospace 9 (8) (2022) 438, http://dx.doi.org/10.3390/aerospace9080438, URL https://www.mdpi.com/2226-4310/9/8/438.

[69] G. Dessena, D.I. Ignatyev, J.F. Whidborne, A. Pontillo, L. Zanotti Fragonara, Ground vibration testing of a high aspect ratio wing with revolving clamp, in: 33rd Congress of the International Council of the Aeronautical Sciences, Stockholm, Sweden, 2022, http://dx.doi.org/10.17862/cranfield.rd.20486229.

[70] S.Y. Yusuf, D. Hayes, A. Pontillo, M.A. Carrizales, G.X. Dussart, M.M. Lone, Aeroelastic scaling for flexible high aspect ratio wings, in: AIAA Scitech 2019 Forum, Kissimmee, FL, 2019, pp. 1–14, http://dx.doi.org/10.2514/6.2019-1594.

[71] I. Tsatsas, A. Pontillo, M. Lone, Aeroelastic damping estimation for a flexible high-aspect-ratio wing, J. Aerosp. Eng. 35 (2) (2022) 1–27, http://dx.doi.org/10.1061/(ASCE)AS.1943-5525.0001390, URL https://ascelibrary.org/doi/10.1061/%28ASCE%29AS.1943-5525.0001390.

A global-local meta-modelling technique for model updating

Dessena, Gabriele

2023-10-09

Dessena G, Ignatyev DI, Whidborne JF, Zanotti Fragonara L. (2024) A global-local meta-modelling technique for model updating, Computer Methods in Applied Mechanics and Engineering, Volume 418, Part A, January 2024, Article Number 116511

https://doi.org/10.1016/j.cma.2023.116511